JOURNAL OF COMPUTATIONAL PHYSICS **130,** 1–24 (1997)
ARTICLE NO. CP965470

On WAF-Type Schemes for Multidimensional Hyperbolic Conservation Laws

S. J. Billett and E. F. Toro

Department of Mathematics and Physics, Manchester Metropolitan University, Chester Street, Manchester M1 5GD, United Kingdom

Received September 11, 1995; revised February 21, 1996

DEDICATED TO JOHN F. CLARKE, FRS, ON THE OCCASION OF HIS SEVENTIETH BIRTHDAY

We explore how the weighted average flux approach can be used to generate first- and second-order accurate finite volume schemes for the linear advection equatons in one, two, and three space dimensions. The derived schemes have multidimensional upwinding aspects and good stability properties. From the two-dimensional methods, we construct a scheme for nonlinear systems of hyperbolic conservation laws that is second-order accurate in smooth flow. Spurious oscillations are controlled by making use of one-dimensional TVD limiter functions. Numerical results are presented for the shallow water equations in two space dimensions. The equivalent schemes are derived for nonlinear systems in three space dimensions.

1. INTRODUCTION

Upwind methods for computational fluid dynamics (CFD) form a respectable class of numerical techniques available to the CFD practitioner today. This is the result of an intensive research activity spanned over many years. The distinguished works of Godunov [9], van Leer [40, 41], Roe [20, 22], Osher and Solomon [18], Harten [11], and many others, have provided a solid theoretical framework for further advancement.

An important issue is how to generalize the first-order Godunov method [9] to second or higher order accuracy. Van Leer [40, 41] proposed his monotone upwind schemes for conservation laws (MUSCL) approach whereby the piecewise constant cell average states in the Godunov method are replaced by reconstructed states that admit spacial variation within each cell. A class of second-order Godunov-type methods based on this approach have been constructed. Examples are the PLM method of Colella [7], the GRP method of Ben-Artzi and Falcovitz [2] and the MUSCL–Hancock scheme [42]. An alternative approach for constructing second-order Godunov type methods is the weighted average flux (WAF) approach [31]. Its origins go back to a random flux approach [30] which was later proved to be second-order accurate in a statistical sense by Toro and Roe [39]. The WAF approach has been shown to be successful in applications to a variety of practical problems [31, 32, 34]. Its key feature is that the second-order accuracy can be achieved by solving the conventional *piecewise constant Riemann problem* as in the first-order Godunov method; no reconstruction/evolution steps are necessary, although these processes may also be admitted. The accuracy comes from utilizing this solution averaged over space and time. This averaging takes the form of an integral of the flux, or chosen variables, over some volume. The WAF method has been extended for use with large timesteps (up to a Courant number of 2) [37, 36] and for use on moving grids [5].

The standard way to extend these schemes to two and three space dimensions is via *space operator splitting*, as discussed by Strang [28], in which the one-dimensional difference operators are used in each dimension in turn. This approach has been shown to be successful: see, for example, the review paper by Woodard and Colella [45]. An important issue is how to extend Godunov-type schemes to two and three dimensions without space splitting. One approach is to use solutions to one-dimensional grid-aligned Riemann problems and one-dimensional operators to construct multidimensional finite volume schemes. This approach has been used to construct the MUSCL–Hancock scheme [19]. A similar approach has been used by LeVeque [16, 17] and Colella [8] to generate finite volume schemes for nonlinear systems, although they account for at least some aspects of multidimensional wave propagation in the construction of their schemes, and as a result their schemes have better stability properties than the MUSCL–Hancock scheme, as will be discussed later. A higher level of upwinding for multidimensional systems of equations is achieved by the so-called *multidimensional upwind* methods. See, for example, Baines [1] or Roe [25, 24]. A good review of multidimensional upwinding has been written by van Leer [43], in which many more references can be found.

In this paper we discuss how the WAF approach can be used to generate finite volume schemes in more than one

0021-9991/97 $25.00

space dimension. We first generalize the approach for the linear advection equation in one space dimension by integrating the exact solution of initial value problems in space and time. We then extend the approach to the two-dimensional linear advection equation and show how different integration methods can lead to numerical schemes with different accuracy and stability properties. In particular, we present two second-order schemes which, as far as we know, are new. They are conservative, finite volume schemes with good stability properties, and are natural extensions of the one-dimensional Lax–Wendroff scheme [14]. Moreover, due to the nature of their derivation, they have multidimensional upwinding features. We also derive a finite volume, first-order scheme that is a natural extension to Godunov's scheme [9] and is the same as Colella's corner upwind transport (CTU) scheme [8] for linear advection. We then construct two schemes for nonlinear systems of hyperbolic conservation laws using the following procedure. We first rewrite the expression for the flux for one of the second-order schemes for the linear advection equation as a sequence of one-dimensional operators. We then add one-dimensional TVD limiter functions to some of these operators to control the spurious oscillations associated with the second-order scheme. When fully limited, the scheme reduces to the first-order CTU scheme. To generate the scheme for nonlinear systems, we then replace the one-dimensional operators by their equivalents for nonlinear systems. The final scheme involves the use of one-dimensional grid-aligned Riemann solvers. Due to both the nature of their derivation and their final form, our schemes lie in the same family of schemes as LeVeque's scheme [16, 17] and Colella's scheme [8]. We derive the equivalent schemes for three-dimensional systems of hyperbolic conservation laws. Some numerical results are presented for the two-dimensional shallow water equations.

This paper is organized as follows: Section 2 introduces the WAF approach and various schemes that it produces in one space dimension. In Section 3 we consider the approach in two space dimensions—we derive finite volume schemes for the linear advection equation, study their accuracy and stability, and construct two schemes for nonlinear systems of hyperbolic conservation laws based on one of the second-order schemes. In Section 4 we derive three-dimensional extensions of the schemes for nonlinear systems. In Section 5 numerical results are presented for the two-dimensional shallow water equations. The paper is summarized in Section 6.

2. THE WAF APPROACH

Consider the model hyperbolic conservation law

$$u_t + f(u)_x = 0, \quad f(u) = au, \tag{1}$$

where u is the conserved variable, $f(u)$ is the physical flux function, and a is the constant speed of convection, assumed positive here. We will consider schemes for (1) that are conservative time marching schemes of the form

$$u_i^{n+1} = u_i^n - \frac{\Delta t}{\Delta x}[f_{i+1/2} - f_{i-1/2}], \tag{2}$$

where $\{u_i^n\}$ is a set of piecewise constant cell averages, Δt and Δx are the time step size and computing cell length, respectively, and $f_{i+1/2}$ is an intercell numerical flux. We define a weighted average flux as

$$f_{i+1/2} = \frac{1}{(t_2 - t_1)} \frac{1}{(x_2 - x_1)} \int_{t_1}^{t_2} \int_{x_1}^{x_2} f(u^*(x,t))\, dx\, dt, \tag{3}$$

where $u^*(x,t)$ is the solution of relevant initial value problems with data $\{u_l^n\}_{l=i-k}^{i+k+1}$. The choice of k depends on the choice of integration range in (3); this is determined by the values of x_1, x_2 and t_1, t_2.

In this section we are exclusively concerned with the choice

$$t_1 = 0, \quad t_2 = \Delta T, \quad x_1 = -\tfrac{1}{2}\Delta x, \quad x_2 = \tfrac{1}{2}\Delta x, \tag{4}$$

where ΔT could be large; that is, the corresponding Courant number

$$\nu = \frac{a\,\Delta T}{\Delta x} \tag{5}$$

could be greater than unity. As the choice of ΔT implies a chosen Courant number, we introduce the notation $\Delta T_{q_1}^{q_2}$ to mean that the associated Courant number ν satisfies $q_1 \le \nu \le q_2$, with q_1, q_2 nonnegative real numbers.

2.1. Exact Integration Schemes

Here we carry out the exact evaluation of integral (3) with choices (4) and $u^*(x, t)$ the solution of piecewise constant Riemann problems.

First consider the case $\Delta T_0^{1/2}$. The integration range, together with the relevant wave pattern, is shown in Fig. 1. It is easy to see that in this case

$$f_{i+1/2} = \tfrac{1}{2}(1 + \nu) f_i + \tfrac{1}{2}(1 - \nu) f_{i+1} \tag{6}$$

which is the familiar Lax–Wendroff flux for the model equation (1). The Lax–Wendroff scheme is second-order accurate in space and time. Figure 2 shows the integration range and wave pattern for $\Delta T_{1/2}^1$. Exact integration produces a three-point flux,

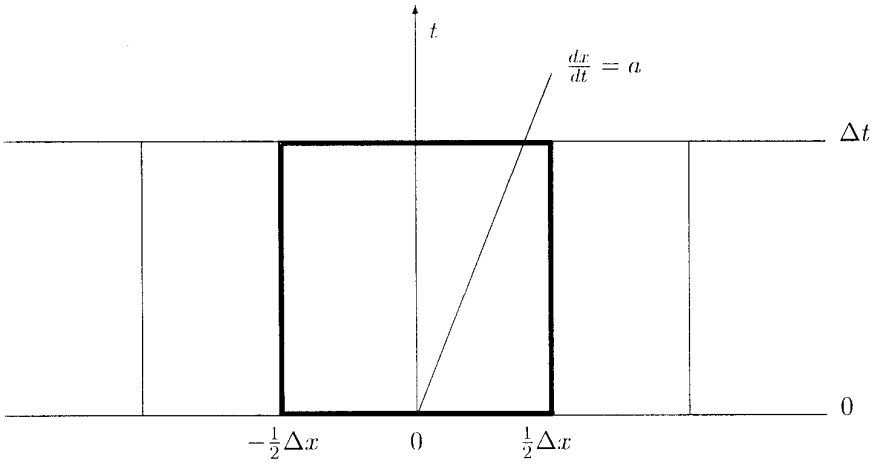

FIG. 1. The integration range and wave structure for $\Delta T_0^{1/2}$.

$$f_{i+1/2} = \frac{1}{8\nu}(2\nu-1)^2 f_{i-1} + \frac{1}{8\nu}(-4\nu^2+12\nu-2) f_i + \frac{1}{8\nu} f_{i+1}. \tag{7}$$

The case $\Delta T_i^{3/2}$ also gives the flux (7). Using (7) in the conservative formula (2) gives the scheme as

$$\begin{aligned} u_i^{n+1} = &-\tfrac{1}{8}u_{i+1}^n + \tfrac{1}{8}(4\nu^2-12\nu+11)u_i^n \\ &-\tfrac{1}{8}(8\nu^2-16\nu+3)u_{i-1}^n + \tfrac{1}{8}(2\nu-1)^2 u_{i-2}^n. \end{aligned} \tag{8}$$

It can be shown (Roe [21]) that a scheme for the linear advection equation (1) of the form

$$u_i^{n+1} = \sum_\alpha A_\alpha u_{i+\alpha}^n \tag{9}$$

is pth order accurate in space and time if and only if

$$\sum_\alpha \alpha^q A_\alpha = (-\nu)^q, \quad 0 \le q \le p. \tag{10}$$

Application of conditions (10) to scheme (8) shows it to be second-order accurate in space and time.

By performing the integration for arbitrary ΔT, we can generate an infinite sequence of schemes. The lth scheme in this sequence is found by integrating with timestep $\Delta T_{q_1}^{q_2}$, where

$$q_1 = l - \tfrac{1}{2}, \quad q_2 = l + \tfrac{1}{2}. \tag{11}$$

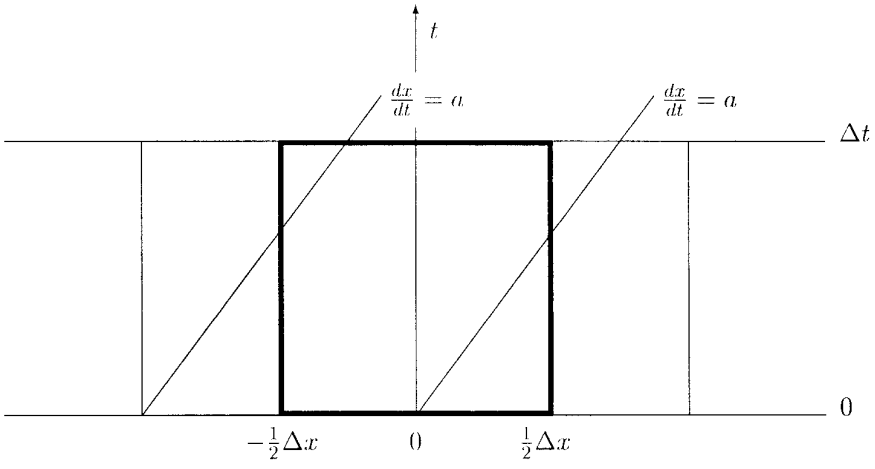

FIG. 2. The integration range and wave structure for $\Delta T_{1/2}^1$.

The cases $l = 0$ and $l = 1$ have been given above. Cases $l \geq 2$ can be derived similarly, and for $l \geq 4$ the intercell flux can be written in the general form

$$f_{i+1/2} = \sum_{k=-l}^{1} W_k f_{i+k}, \tag{12}$$

where

$$\begin{aligned} W_1 &= \frac{1}{8\nu} \\ W_0 &= \frac{7}{8\nu} \\ W_k &= \frac{1}{\nu}, \quad k \in \{2 - l \ldots -1\} \\ W_{1-l} &= \frac{1}{\nu}\left[1 - \frac{1}{8}(2(\nu - l) - 1)^2\right] \\ W_{-l} &= \frac{1}{8\nu}(2(\nu - l) + 1)^2. \end{aligned} \tag{13}$$

Substituting the flux (13) into the conservative formula (2) gives the scheme for general l; application of accuracy conditions (10) to this scheme shows it to be second-order accurate in space and time for all l.

Now consider the stability of the above schemes. The scheme $l = 0$ is the Lax–Wendroff scheme, and it is well known that this is stable, provided $\nu \leq 1$. We have not managed to formally derive stability limits for any cases $l \geq 1$; however, plotting the von Neumann amplification factor for various schemes in the sequence, at various Courant numbers, suggests that the lth scheme, $l \geq 1$, is stable whenever

$$l - \frac{1}{\sqrt{2}} \leq \nu \leq l + \frac{1}{\sqrt{2}}. \tag{14}$$

2.2. Approximate Integration Schemes

Formula (3) with restriction (4) becomes

$$f_{i+1/2} = \frac{1}{\Delta T}\frac{1}{\Delta x}\int_0^{\Delta T}\int_{-\Delta x/2}^{\Delta x/2} f(u^*(x,t))\,dx\,dt. \tag{15}$$

We now study schemes that can be generated from this general flux if approximate integration methods are used. Use of the midpoint rule in space gives

$$f_{i+1/2} = \frac{1}{\Delta T}\int_0^{\Delta T} f(u^*(0,t))\,dt \tag{16}$$

which is the usual time-average intercell flux evaluation along the t-axis in the solution of the Riemann problem. If $u^*(x,t)$ is taken to represent the solution of the conventional piecewise constant Riemann problem with data u_i^n, u_{i+1}^n and a timestep ΔT_0^1 is used then the first-order Godunov method is reproduced. If reconstructed (sloped) data is introduced, various MUSCL-type schemes can be reproduced, such as the generalised Riemann problem (GRP) method of Ben-Artzi and Falcovitz [2] or the piecewise linear method (PLM) of Colella [7]. See [38] for a further discussion.

A midpoint rule in time applied to (15) gives

$$f_{i+1/2} = \frac{1}{\Delta x}\int_{-\Delta x/2}^{\Delta x/2} f\left(u^*\left(x, \frac{1}{2}\Delta t\right)\right)dx. \tag{17}$$

Here we assume u^* is the exact solution of the piecewise constant Riemann problem. Exact space integration, for ΔT_0^1, again gives the Lax–Wendroff flux (6) for (1). This observation formed the basis for the original WAF method [31, 34] for nonlinear systems, which we describe in the next section, since it will be useful later. For ΔT_1^2 exact integration in (17) gives

$$f_{i+1/2} = \tfrac{1}{2}(\nu - 1) f_{i-1} + \tfrac{1}{2}(3 - \nu) f_i \tag{18}$$

which is the flux for the Warming–Beam second-order upwind method [44]. This is stable provided $0 \leq \nu \leq 2$. Toro and Billett [37, 36] have derived a TVD scheme that uses (6) for $0 \leq \nu \leq 1$ and (18) for $1 \leq \nu \leq 2$. This scheme has a CFL stability limit of 2 and was extended for solving nonlinear systems of hyperbolic conservation laws in [37, 36]. The resulting scheme was tested on the Euler equations of gas dynamics in one space dimension and in two space dimensions via operator splitting, and it proved successful.

2.3. The WAF Method for Systems of Equations

Consider the nonlinear system of conservation laws

$$\mathbf{U}_t + \mathbf{F}(\mathbf{U})_x = 0, \tag{19}$$

where $\mathbf{U}$ is a vector of N conserved variables and $\mathbf{F}(\mathbf{U})$ is a vector valued flux function. We assume the system is *strictly hyperbolic*; i.e., the matrix $A = \partial\mathbf{F}/\partial\mathbf{U}$ has N real and distinct eigenvalues. The conservative formula for such systems is

$$\mathbf{U}_i^{n+1} = \mathbf{U}_i^n - \frac{\Delta t}{\Delta x}[\mathbf{F}_{i+1/2} - \mathbf{F}_{i-1/2}], \tag{20}$$

where $\mathbf{U}_i^n$ is the integral average of $\mathbf{U}$ in cell i at timelevel n and $\mathbf{F}_{i+1/2}$ is an intercell numerical flux. The integral (17) for $f_{i+1/2}$ is reinterpreted for $\mathbf{F}_{i+1/2}$ as an integral across

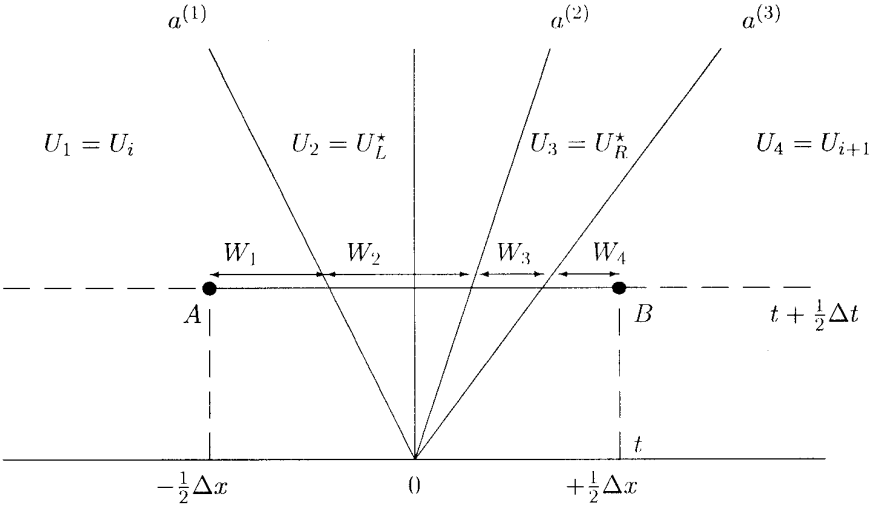

FIG. 3. Weights W_k for the WAF scheme on a system of $N = 3$ equations.

a local Riemann problem for (19), i.e., system (19) with initial conditions

$$\mathbf{U}_0(x) = \begin{cases} \mathbf{U}_i^n & \text{if } x < 0, \\ \mathbf{U}_{i+1}^n & \text{otherwise.} \end{cases} \tag{21}$$

We refer to this Riemann problem as RP($\mathbf{U}_i^n$, $\mathbf{U}_{i+1}^n$). The solution to RP($\mathbf{U}_i^n$, $\mathbf{U}_{i+1}^n$) consists of N waves with speeds $a_{i+1/2}^{(k)}$ separating $N + 1$ constant states, which we denote by $\mathbf{U}_{i+1/2}^{(k)}$, $1 \le k \le N + 1$. Note that $\mathbf{U}_{i+1/2}^{(1)} \equiv \mathbf{U}_i^n$ and $\mathbf{U}_{i+1/2}^{(N+1)} \equiv \mathbf{U}_{i+1}^n$. The solution is self-similar; i.e., it is only a function of the similarity variable $\zeta = x/t$ and can thus be denoted $\overline{\mathbf{U}}_{i+1/2}(\zeta)$. The flux can be written as

$$\mathbf{F}_{i+1/2} = \frac{1}{\Delta x} \int_{-\Delta x/2}^{\Delta x/2} \mathbf{F}\left(\overline{\mathbf{U}}\left(\frac{x}{\Delta t/2}\right)\right) dx. \tag{22}$$

In practice, it is sufficient to represent all waves in the solution as *single ray waves*; the integral (22) then becomes a weighted average of the fluxes in the solution to the Riemann problem:

$$\mathbf{F}_{i+1/2} = \sum_{k=1}^{N+1} W^{(k)} \mathbf{F}_{i+1/2}^{(k)}, \tag{23}$$

where $\mathbf{F}_{i+1/2}^{(k)}$ is the kth flux in the solution of the Riemann problem. The weights $W^{(k)}$ are

$$W^{(k)} = \tfrac{1}{2}(\nu_{i+1/2}^{(k)} - \nu_{i+1/2}^{(k-1)}), \tag{24}$$

where $\nu_{i+1/2}^{(k)} = a_{i+1/2}^{(k)} \Delta t/\Delta x$, $k = 1, ..., N$, is the Courant–Friedrichs–Lewy (CFL) number of the kth wave, $a_{i+1/2}^{(k)}$ is the speed of the kth wave, and

$$\nu_{i+1/2}^{(0)} = -1, \quad \nu_{i+1/2}^{(N+1)} = +1.$$

See Fig. 3 for an example of the case $N = 3$. These weights give a scheme that is second-order accurate in space and time and thus suffers from spurious oscillations. In practice, therefore, the weights (24) are replaced by

$$W^{(k)} = \tfrac{1}{2}(\phi_{i+1/2}^{(k)} - \phi_{i+1/2}^{(k-1)}) \tag{25}$$

with

$$\phi_{i+1/2}^{(0)} = -1, \quad \phi_{i+1/2}^{(N-1)} = +1.$$

The functions $\phi_{i+1/2}^{(k)} = \text{sgn}(\nu_{i+1/2}^{(k)}) \overline{\phi}_{i+1/2}^{(k)}$ are total variation diminishing (TVD) *limiter functions*, used to control the spurious oscillations associated with second-order schemes. Limiter functions depend on the local Courant numbers $\nu_{i+1/2}^{(k)}$ and a local *flow parameter* $r_{i+1/2}^{(k)}$,

$$r_{i+1/2}^{(k)} = \frac{\Delta q_{\text{upw}}}{\Delta q_{\text{loc}}}, \tag{26}$$

where q is some suitable variable. Here Δq_{loc} is the *local* jump in q,

$$\Delta q_{\text{loc}} = q_{i+1/2}^{(k+1)} - q_{i+1/2}^{(k)},$$

and Δq_{upw} is the *upwind* jump,

$$\Delta q_{\text{upw}} = \begin{cases} q_{i-1/2}^{(k+1)} - q_{i-1/2}^{(k)} & \text{if } \nu_{i+1/2}^{(k)} > 0 \\ q_{i+3/2}^{(k+1)} - q_{i+3/2}^{(k)} & \text{if } \nu_{i+1/2}^{(k)} < 0. \end{cases}$$

For most waves, q can be taken as density for the Euler equations or geopotential for the shallow water equations. For waves across which these variables do not change, other variables must be used—for example the tangential

component of velocity can be used across shear waves. Note that $r_{i+1/2}^{(k)} \approx 1$ corresponds to gradients in q that vary slowly in space, and $r_{i+1/2}^{(k)} \approx 0$ corresponds to rapid increase in the magnitude of the gradient of q in the direction of wave propagation. It is in this latter case that second (and higher) order schemes produce spurious oscillations in the solution. WAF, as all other TVD schemes, will avoid these oscillations by adding numerical dissipation via the limiter functions. The extreme case is $r_{i+1/2}^{(k)} = 0\ \forall k$, in which case the WAF intercell flux at boundary $i + \frac{1}{2}$ reduces to the Godunov first-order intercell flux. Limiter functions ϕ are related to the well-known flux limiters B of Roe [23] via

$$\overline{\phi} = 1 - (1 - |\nu|)B.$$

A popular limiter function arising from TVD conditions is the van Leer limiter

$$\overline{\phi}(r, \nu) = \begin{cases} 1, & r \le 0, \\ 1 - 2(1 - |\nu|)r/(1 + r), & r > 0, \end{cases} \tag{27}$$

where we have dropped subscripts and superscripts for convenience. See [31, 34, 35] for further discussion about the WAF method applied to nonlinear systems and the derivation of the TVD limiter functions.

3. THE WAF APPROACH IN TWO SPACE DIMENSIONS

In this section we show how the WAF approach, as discussed in the last section, can be used to generate two-dimensional finite volume schemes. Our aim is to illustrate the approach, rather than provide an exhaustive account of all possibilities. Therefore, after defining an intercell flux for the general case, we restrict ourselves to regular, Cartesian grids, assume the data is constant within each cell, and consider only Courant numbers less than unity. Applications to curvilinear or unstructured grids are, of course, also possible, as well as MUSCL-type schemes, and 'large timestep' schemes, but we do not consider these here.

We will first consider the linear advection equation and explore the schemes that can be generated from combinations of exact integration and the midpoint rule in space and time. We study their accuracy and stability. We then show how two of the schemes, one first order and one second order, can be combined and generalized to nonlinear systems of hyperbolic conservation laws to produce a scheme that is second-order accurate in space and time away from high gradients, and almost monotonicity preserving in regions of high gradient. Numerical results are presented for this scheme applied to the shallow water equations in Section 5.

In two space dimensions the linear advection equation can be written as

$$u_t + f_x + g_y = 0, \tag{28}$$

where $f = au$ and $g = bu$ are flux components, a and b are components of the velocity vector (a, b), assumed constant and positive here, and (x, y) are two space coordinates. It has the exact solution

$$u(x, y, t) = u^{(0)}(x - at, y - bt) \tag{29}$$

for given initial conditions $u^{(0)}(x, y)$.

For a general grid (structured or unstructured), we can define a general WAF intercell flux $\mathbf{e}_{AB}$ for boundary AB as

$$\mathbf{e}_{AB} = \frac{1}{t_2 - t_1} \frac{1}{V(I)} \int_{t_1}^{t_2} \int_I \mathbf{e} \cdot \mathbf{n}\, dx\, dy\, dt, \tag{30}$$

where I is a space integration range in (x, y), $V(I)$ is the area of I, $\mathbf{e} = (au, bu)$ is the general flux function, and $\mathbf{n}$ is the unit outward facing vector normal to the intercell boundary.

3.1. Two-Dimensional Schemes for Cartesian Grids

We consider here the simple case of regular Cartesian grids. Let Δx, Δy be the mesh spacings, let Δt be the timestep, and assume that a and b are constant and positive. Consider the two-dimensional conservation formula

$$u_{i,j}^{n+1} = u_{i,j}^n - \frac{\Delta t}{\Delta x}[f_{i+1/2,j} - f_{i-1/2,j}] - \frac{\Delta t}{\Delta y}[g_{i,j+1/2} - g_{i,j-1/2}], \tag{31}$$

where $u_{i,j}^n$ is the integral average of u in cell (i, j) at time level n and $f_{i+1/2,j}$ and $g_{i,j+1/2}$ are intercell fluxes in the x and y directions, respectively. When applied to Cartesian grids, the formula (30) gives intercell fluxes in the x-direction as

$$f_{i+1/2,j} = \frac{1}{t_2 - t_1} \frac{1}{V(I)} \int_{t_1}^{t_2} \int_I f(u^*(x, y, t))\, dx\, dy\, dt, \tag{32}$$

where $u^*(x, y, t)$ is the solution to the initial value problem for (28) with initial data u^n at time level n. The fluxes in the y-direction follow by symmetry. Define the Courant numbers in the x and y directions as $\nu_x = a\Delta t/\Delta x$ and $\nu_y = b\Delta t/\Delta y$, respectively. We consider here only the case when the time limits are $t_1 = 0$ and $t_2 = \Delta t$, where Δt is the timestep chosen such that $\nu_x \le 1$ and $\nu_y \le 1$. For the flux $f_{i+1/2,j}$ we always take the space integration range as

$$I = [-\tfrac{1}{2}\Delta x, \tfrac{1}{2}\Delta x] \times [0, \Delta y], \tag{33}$$

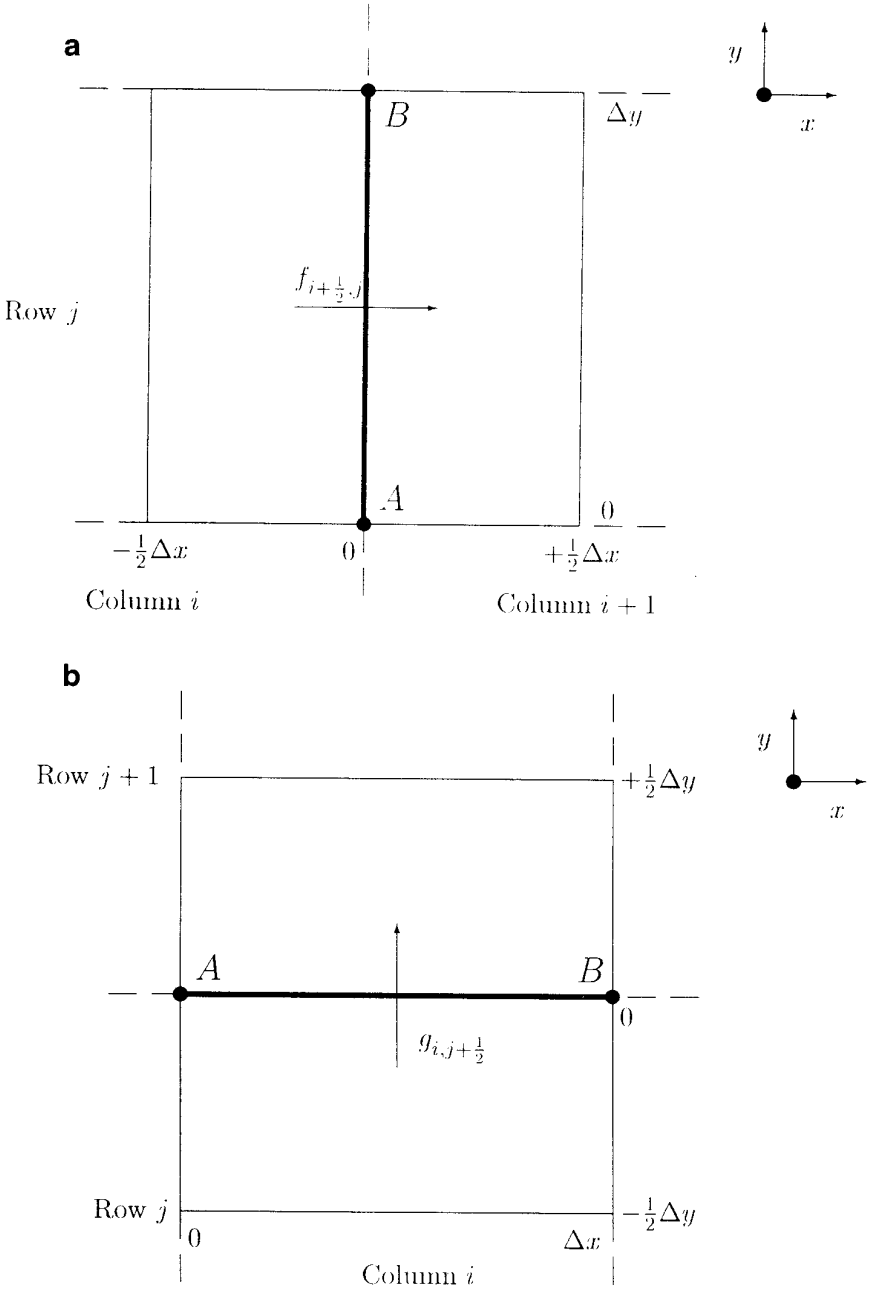

FIG. 4. Space integration ranges for (a) the fluxes $f_{i+1/2,j}$, and (b) the fluxes $g_{i,j+1/2}$.

where, in local coordinates, $x = 0$ lies on the boundary, and $y = 0$, $y = \Delta y$ lie on the ends of the boundary. For the flux $g_{i,j+1/2}$ the obvious changes are made. See Fig. 4. Many other integration ranges are possible, but are not considered here:

This choice of Courant numbers and integration range restricts the number of states that influence $f_{i+1/2,j}$ to four: $u^n_{i,j}$, $u^n_{i+1,j}$, $u^n_{i,j-1}$ and $u^n_{i+1,j-1}$. These are laid out in the four quadrants of a rectangle, and form the initial conditions of a two dimensional Riemann problem.

3.1.1. *Exact Integration in All Directions*

Consider first the case of exact integration in time and both space directions. We assume that $\nu_x \leq \frac{1}{2}$ and $\nu_y \leq \frac{1}{2}$ to restrict the number of waves entering the integration range. At any given point (x, y) in I, and at any $t \in [t^n, t^n+1]$, we know the exact value of the flux in the solution to the initial value problem with initial data $u(x, y, t^n)$ is

$$f(x, y, t) = f(u(x - a(t - t^n), y - b(t - t^n), t^n)).$$

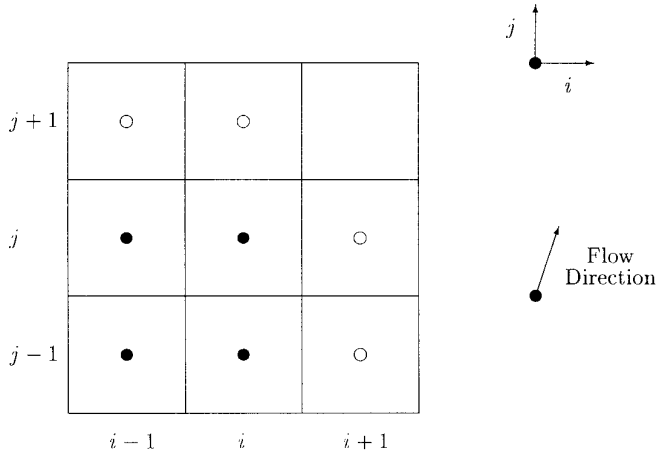

FIG. 5. The stencil for the second-order schemes: full circles denote upwind points, empty circles denote downwind points.

To obtain our intercell flux, we integrate this flux function through space and time. This gives the intercell flux $f_{i+1/2,j}$ as

$$\begin{aligned} f_{i+1/2,j} &= \tfrac{1}{12}[6 + 6\nu_x - 3\nu_y - 4\nu_x\nu_y]f_{i,j} \\ &\quad + \tfrac{1}{12}[6 - 6\nu_x - 3\nu_y + 4\nu_x\nu_y]f_{i+1,j} \\ &\quad + \tfrac{1}{12}[3\nu_y + 4\nu_x\nu_y]f_{i,j-1} + \tfrac{1}{12}[3\nu_y - 4\nu_x\nu_y]f_{i+1,j-1}, \end{aligned} \tag{34}$$

where $f_{i,j} = f(u^n_{i,j}) = au^n_{i,j}$. The intercell flux $g_{i,j+1/2}$ follows by symmetry. Substituting both $f_{i+1/2,j}$ and $g_{i,j+1/2}$ into the conservative formula (31) gives the full scheme as

$$\begin{aligned} u^{n+1}_{i,j} &= [1 - \nu_x^2 - \nu_y^2 + \tfrac{2}{3}\nu_x\nu_y(\nu_x + \nu_y)]u^n_{i,j} \\ &\quad + \tfrac{1}{12}\nu_y[6(\nu_y - 1) + \nu_x(3 - 4\nu_y)]u^n_{i,j+1} \\ &\quad + \tfrac{1}{12}\nu_x[6(\nu_x - 1) + \nu_y(3 - 4\nu_x)]u^n_{i+1,j} \\ &\quad + \tfrac{1}{12}\nu_x\nu_y(4\nu_x - 3)u^n_{i+1,j-1} \\ &\quad + \tfrac{1}{12}\nu_x\nu_y(4\nu_y - 3)u^n_{i-1,j+1} \\ &\quad + \tfrac{1}{12}\nu_y[6(1 + \nu_y) - \nu_x(3 + 4\nu_y + 8\nu_x)]u^n_{i,j-1} \\ &\quad + \tfrac{1}{12}\nu_x[6(1 + \nu_x) - \nu_y(3 + 4\nu_x + 8\nu_y)]u^n_{i-1,j} \\ &\quad + \tfrac{1}{12}\nu_x\nu_y[6 + 4(\nu_x + \nu_y)]u^n_{i-1,j-1}. \end{aligned} \tag{35}$$

This scheme has an eight-point stencil with both upwind and downwind components, as shown in Fig. 5. Note that when $\nu_x = 0$ or $\nu_y = 0$, the scheme reduces to the one-dimensional Lax–Wendroff scheme. It can be shown, via truncation error analysis, that schemes for the solution of the two-dimensional linear advection equation (28) on regular Cartesian grids of the form

$$u^{n+1}_{i,j} = \sum_{\alpha,\beta} A_{\alpha,\beta}u^n_{i+\alpha,j+\beta} \tag{36}$$

are pth-order accurate in space and time if and only if

$$\sum_{\alpha,\beta} \alpha^q\beta^r A_{\alpha,\beta} = (-\nu_x)^q(-\nu_y)^r \tag{37}$$

for all integer pairs (q, r) such that $q \geq 0$, $r \geq 0$, and $q + r \leq p$. See [4] for proof. Applying conditions (37) to scheme (35) shows it to be second-order accurate in space and time. Although we assume $\nu_x \leq \frac{1}{2}$ and $\nu_y \leq \frac{1}{2}$ in the derivation of the scheme, we anticipate that the stability condition for this scheme is

$$\nu_x^2 + \nu_y^2 \leq 1. \tag{38}$$

See Section 3.1.5 for further discussion of this stability condition.

3.1.2. *The Midpoint Rule in Space*

We now consider the schemes generated by using exact integration in time and the midpoint rule in space in (32). We again assume that $\nu_x \leq \frac{1}{2}$ and $\nu_y \leq \frac{1}{2}$.

Consider first exact integration in time, the midpoint rule perpendicular to the boundary, and exact integration parallel to the boundary. The integral form of the intercell flux (32) simplifies in this case to

$$f_{i+1/2,j} = \frac{1}{\Delta t}\frac{1}{\Delta y}\int_0^{\Delta t}\int_{I\cap\{x=0\}} f(u^*(0, y, t))\, dy\, dt, \tag{39}$$

where we integrate over the plane $x = 0$. This gives the intercell flux $f_{i+1/2,j}$ as

$$f_{i+1/2,j} = \tfrac{1}{2}(2 - \nu_y)f_{i,j} + \tfrac{1}{2}\nu_y f_{i,j-1}. \tag{40}$$

The scheme resulting from this flux is

$$\begin{aligned} u^{n+1}_{i,j} &= (1 - \nu_x - \nu_y + \nu_x\nu_y)u^n_{i,j} + \nu_y(1 - \nu_x)u^n_{i,j-1} \\ &\quad + \nu_x(1 - \nu_y)u^n_{i-1,j} + \nu_x\nu_y u^n_{i-1,j-1}. \end{aligned} \tag{41}$$

Conditions (37) show this scheme to be first-order accurate in space and time. It is the corner transport upwind (CTU) scheme of Colella [8] on (28). Colella proved this scheme to be stable, provided

$$\max\{\nu_x, \nu_y\} \leq 1. \tag{42}$$

Use of exact integration in time, the midpoint rule parallel to the boundary, and exact integration perpendicular to the boundary leads to an unconditionally unstable scheme.

Use of exact integration in time and the midpoint rule

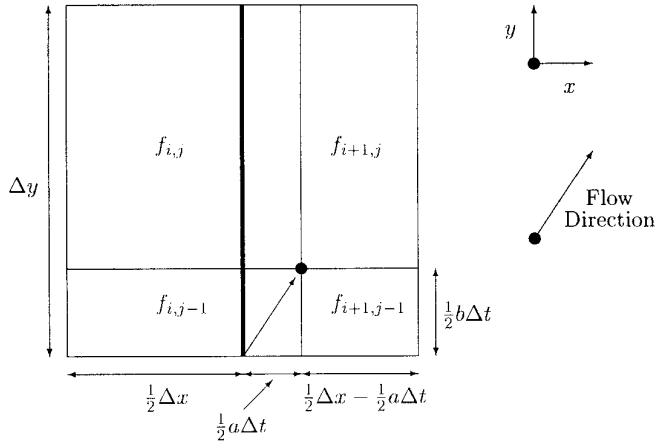

FIG. 6. Integration using midpoint rule in time and exact integration in both space directions: status of the space integration range at time $t = \frac{1}{2}\Delta t$.

in both space dimensions leads to the one-dimensional Godunov flux on each boundary. The resulting scheme is first-order accurate and stable, provided $\nu_x + \nu_y \le 1$, as is well known.

3.1.3. *The Midpoint Rule in Time*

We now consider the midpoint rule in time combined with exact integration in both space directions and assume that $\nu_x \le 1$ and $\nu_y \le 1$. The integral form of the intercell flux (32) simplifies in this case to

$$f_{i+1/2,j} = \frac{1}{\Delta x\,\Delta y}\int_I f\left(u^*\left(x, y, \frac{1}{2}\Delta t\right)\right) dx\,dy; \qquad (43)$$

i.e., we integrate over the plane $t = \frac{1}{2}\Delta t$. See Fig. 6. This gives intercell flux:

$$\begin{aligned} f_{i+1/2,j} = {} & \tfrac{1}{4}(1+\nu_x)(2-\nu_y) f_{i,j} + \tfrac{1}{4}(1-\nu_x)(2-\nu_y) f_{i+1,j} \\ & + \tfrac{1}{4}(1+\nu_x)\nu_y f_{i,j-1} + \tfrac{1}{4}(1-\nu_x)\nu_y f_{i+1,j-1}. \end{aligned} \qquad (44)$$

The flux $g_{i,j+1/2}$ follows similarly. Substituting both fluxes into the conservative scheme (31) gives the scheme in full form as

$$\begin{aligned} u_{i,j}^{n+1} = {} & [1 - \tfrac{1}{2}\nu_x^2(2-\nu_y) - \tfrac{1}{2}\nu_y^2(2-\nu_x)] u_{i,j}^n \\ & - \tfrac{1}{4}\nu_x(1-\nu_x)(2-\nu_y) u_{i+1,j}^n \\ & - \tfrac{1}{4}(2-\nu_x)\nu_y(1-\nu_y) u_{i,j+1}^n \\ & - \tfrac{1}{4}\nu_x\nu_y(1-\nu_x) u_{i+1,j-1}^n - \tfrac{1}{4}\nu_x\nu_y(1-\nu_y) u_{i-1,j+1}^n \\ & + \tfrac{1}{4}[\nu_x(1+\nu_x)(2-\nu_y) - 2\nu_x\nu_y^2] u_{i-1,j}^n \\ & + \tfrac{1}{4}[\nu_y(1+\nu_y)(2-\nu_x) - 2\nu_x^2\nu_y] u_{i,j-1}^n \\ & + \tfrac{1}{4}\nu_x\nu_y(2+\nu_x+\nu_y) u_{i-1,j-1}^n. \end{aligned} \qquad (45)$$

This scheme has the eight-point compact stencil shown in Fig. 5. When $\nu_x = 0$ or $\nu_y = 0$, the scheme reduces to the one-dimensional Lax–Wendroff scheme, and when $\nu_x = \nu_y = 1$, it reduces to

$$u_{i,j}^{n+1} = u_{i-1,j-1}^n \qquad (46)$$

which reproduces the exact solution under the given initial conditions. Application of conditions (37) to scheme (45) shows that it is second-order accurate in space and time. We anticipate that this scheme is stable, provided (42) holds. See Section 3.1.5 for a further discussion of stability.

3.1.4. *The Midpoint Rule in Both Space and Time*

We now consider the schemes generated by using the midpoint rule in time and combinations of exact integration and the midpoint rule in space. We again assume that $\nu_x \le 1$ and $\nu_y \le 1$. As in Section 3.1.2, there are three cases to consider: the midpoint rule parallel to the boundary and exact integration perpendicular to the boundary; the midpoint rule perpendicular to the boundary and exact integration parallel to the boundary; and the midpoint rule in both directions. These three cases will result in the same schemes as in Section 3.1.2.

3.1.5. *Stability of the Second-Order Schemes*

We have not managed to perform rigorous stability analysis on the two new second-order schemes (35) and (45). However, a good indication of the stability of a scheme can be found by computing the von Neumann amplification coefficient A for a large number of quadruples (ν_x, ν_y, θ, ϕ), where θ and ϕ are the phase angles in the x and y directions, respectively. We can define $st(\nu_x, \nu_y)$ to be the ratio of stable pairs (θ, ϕ) for given (ν_x, ν_y), i.e., the number for which $|A| \le 1$, to the total number tested. The scheme is only stable for the pair (ν_x, ν_y) if $st(\nu_x, \nu_y) = 1$, i.e., if all Fourier modes are stable. Figure 7 shows contour plots of $st(\nu_x, \nu_y)$ against (ν_x, ν_y) when $\nu_x \le 2$ and $\nu_y \le 2$ for schemes (35) and (45).

Figure 7a is the plot for the scheme (35) derived using exact integration in all directions in Section 3.1.1. It suggests that the scheme is stable whenever (38) holds. Recall that the scheme is also second-order accurate in space and time and a two-dimensional extension of the Lax–Wendroff scheme. Figure 7b is the plot for the second-order accurate scheme (45) derived using the midpoint rule in time and exact integration in both space dimensions in Section 3.1.3. It indicates that the scheme has stability condition (42).

We have applied the above approach to stability analysis to various second-order schemes on the two-dimensional linear advection equation. LeVeque's scheme [16, 17] and Colella's scheme [8] were found to be stable, provided (42)

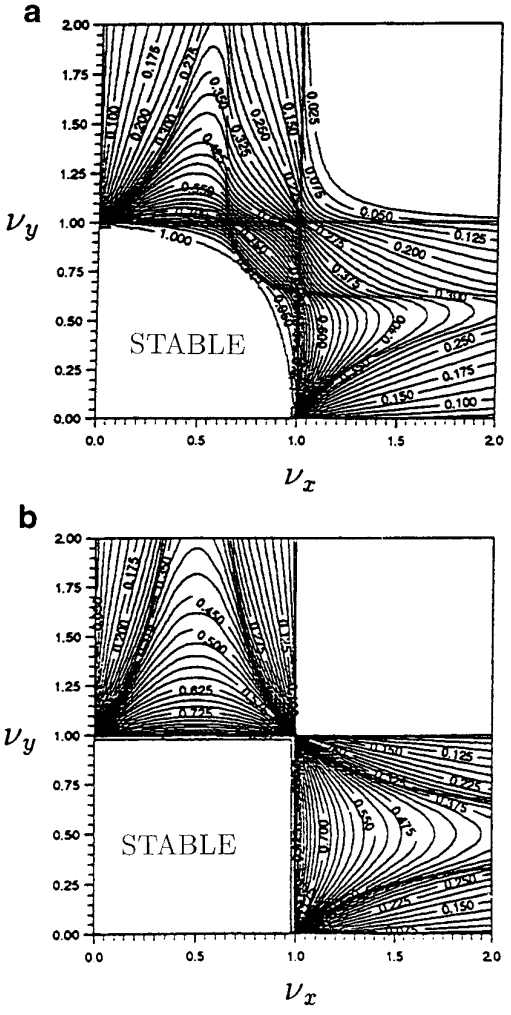

FIG. 7. Ratio of the number of stable phase angle pair to the total number of phase angle pairs for the two-dimensional second-order schemes. (a) is the plot for Scheme (35), and (b) is the plot for Scheme (45).

holds. Application of this technique to the two-dimensional MUSCL–Hancock scheme [19], with central differencing used in the piece-wise linear data reconstruction, indicates that it is stable only if

$$\nu_x + \nu_y \leq 1. \tag{47}$$

Thus the second-order WAF schemes appear to have better stability properties than the MUSCL–Hancock scheme with this reconstruction and comparable stability to LeVeque's scheme [16, 17] and Colella's scheme [8]. They are much more stable than the "traditional" Lax–Wendroff scheme [15] in two dimensions, which is restricted by the condition

$$\nu_x^2 + \nu_y^2 \leq \tfrac{1}{8} \tag{48}$$

3.2. Schemes for Nonlinear Systems

We now discuss WAF-type schemes for two-dimensional nonlinear systems of hyperbolic conservation laws. Recall that schemes for the linear advection equation (28) were obtained from the exact solution to two-dimensional Riemann problems. While there have been some advances in the development of exact solvers for multidimensional Riemann problems [46, 26] such solvers do not appear to have matured enough to be of use in the construction of multidimensional schemes, and even if such solvers were available the resulting schemes are likely to be too complicated for common use. Therefore, we do not apply the WAF approach directly for nonlinear systems, but instead we reinterpret the numerical flux (44) for the linear advection equation (28) to produce extensions of scheme (45). We consider two extensions: an "average flux" scheme and an "average state" scheme.

3.2.1. *An Average Flux Scheme*

The intercell flux (44) can be written as

$$\begin{aligned} f_{i+1/2,j} = &\frac{1}{2}(1+\nu_x) f\left(u_{i,j} - \frac{\Delta t/2}{\Delta x}\left[\bar{g}_{i,j+1/2} - \bar{g}_{i,j-1/2}\right]\right) \\ &+ \frac{1}{2}(1-\nu_x) f\left(u_{i+1,j} - \frac{\Delta t/2}{\Delta x}\left[\bar{g}_{i+1,j+1/2} - \bar{g}_{i+1,j-1/2}\right]\right), \end{aligned} \tag{49}$$

where $\bar{g}_{i,j+1/2} = bu_{i,j}$. The flux in this form motivates us to define the following operators. First, define two Godunov operators along strips of cells

$$\mathbf{L}^{\mathrm{GOD}}_{x,dt}(\mathbf{Z}^n_{i,j}) = \mathbf{Z}^n_{i,j} - \frac{\Delta t}{\Delta x}\left[\mathbf{F}^{\mathrm{GOD}}_{i+1/2,j} - \mathbf{F}^{\mathrm{GOD}}_{i-1/2,j}\right], \tag{50}$$

where $\mathbf{F}^{\mathrm{GOD}}_{i+1/2,j}$ is a Godunov intercell flux in the x-direction, and

$$\mathbf{L}^{\mathrm{GOD}}_{y,dt}(\mathbf{Z}^n_{i,j}) = \mathbf{Z}^n_{i,j} - \frac{\Delta t}{\Delta y}\left[\mathbf{G}^{\mathrm{GOD}}_{i,j+1/2} - \mathbf{G}^{\mathrm{GOD}}_{i,j-1/2}\right], \tag{51}$$

where $\mathbf{G}^{\mathrm{GOD}}_{i,j+1/2}$ is a Godunov intercell flux in the y-direction. Here, $\mathbf{Z}^n$ is some state at timelevel n indexed by (i, j), such as $u^n_{i,j}$. The parameter dt is a timestep, which is usually to be taken as $dt = \Delta t$ or $dt = \frac{1}{2}\Delta t$, although any other stable timestep could be used. This form of the operator $\mathbf{L}^{\mathrm{GOD}}_{s,dt}$ appears twice in (49). The second operator we define here computes a WAF intercell flux based on the solution to the Riemann problem for two given states $\mathbf{Z}_L$ and $\mathbf{Z}_R$,

$$\mathbf{L}^{\mathrm{WAF}}_{s,dt}(\mathbf{Z}_L, \mathbf{Z}_R) = \frac{1}{\Delta s}\int_{-\Delta s/2}^{\Delta s/2} \mathbf{E}\left(\mathbf{Z}^*\left(\frac{s}{dt}\right)\right) ds, \tag{52}$$

where $\mathbf{Z}^*$ is the solution to RP($\mathbf{Z}_L, \mathbf{Z}_R$) and $\mathbf{E}$ is the flux in direction s. In practice, all waves in the solution to RP($\mathbf{Z}_L, \mathbf{Z}_R$) would be represented by single ray waves and the operator can be written as a weighted average of the fluxes $\mathbf{E}^{(k)}$ in the solution to the Riemann problem:

$$\mathbf{L}^{\mathrm{WAF}}_{s,dt}(\mathbf{Z}_L, \mathbf{Z}_R) = \sum_{k=1}^{N+1} W^{(k)} \mathbf{E}^{(k)}. \tag{53}$$

The weights $W^{(k)}$ are taken as the weights (25) for the TVD version of the one dimensional WAF scheme. In the present notation they are written

$$W^{(k)} = \phi^{(k)} - \phi^{(k-1)}, \quad \phi^{(0)} = -1, \quad \phi^{(N+1)} = 1, \tag{54}$$

where $\phi^{(k)}$ is a limiter function for the kth wave. Note that for the linear advection equation with the limiter function $\phi^{(k)} \equiv \nu_s$ for $s = x$ and $dt = \frac{1}{2}\,\Delta t$, $\mathbf{L}^{\mathrm{WAF}}_{s,dt}\,(u_L, u_R)$ becomes

$$\mathbf{L}^{\mathrm{WAF}}_{x,\Delta t/2}(u_L, u_R) = \tfrac{1}{2}(1 + \nu_x) f(u_L) + \tfrac{1}{2}(1 - \nu_x) f(u_R). \tag{55}$$

for non-Cartesian geometries with body-fitted grids $\mathbf{L}^{\mathrm{GOD}}_{s,dt}$ and $\mathbf{L}^{\mathrm{WAF}}_{s,dt}$ are reinterpreted in the obvious way. We can write flux (49) in terms of operators as

$$f_{i+1/2,j} = \mathbf{L}^{\mathrm{WAF}}_{x,\Delta t/2}(\mathbf{L}^{\mathrm{GOD}}_{y,\Delta t/2}(u^n_{i,j}), \mathbf{L}^{\mathrm{GOD}}_{y,\Delta t/2}(u^n_{i,j})). \tag{56}$$

Similarly we define a flux $g_{i,j+1/2}$ as

$$g_{i,j+1/2} = \mathbf{L}^{\mathrm{WAF}}_{y,\Delta t/2}(\mathbf{L}^{\mathrm{GOD}}_{x,\Delta t/2}(u^n_{i,j}), \mathbf{L}^{\mathrm{GOD}}_{x,\Delta t/2}(u^n_{i,j+1})). \tag{57}$$

The use of limiter functions in the WAF operator $\mathbf{L}^{\mathrm{WAF}}_{s,dt}$ does not make the scheme TVD, but numerical experiments have shown that the limiter functions do control the spurious oscillations associated with the second-order scheme. By the results of Goodman and LeVeque [10], a TVD version of the scheme would be at most first-order accurate and thus too diffusive for practical applications. See [6] for a total variation bounded (TVB) version of the scheme for the linear advection equation. The TVB scheme has not yet been extended to systems of equations.

Consider nonlinear hyperbolic systems of equations

$$\mathbf{U}_t + \mathbf{F}(\mathbf{U})_x + \mathbf{G}(\mathbf{U})_y = 0 \tag{58}$$

where $\mathbf{U}$ is a vector on N conserved variables and $\mathbf{F}$ and $\mathbf{G}$ are vector-valued flux functions. The method we propose here for the solution of (58) will be written in conservation form

$$\mathbf{U}^{n+1}_{i,j} = \mathbf{U}^n_{i,j} - \frac{\Delta t}{\Delta x}[\mathbf{F}_{i+1/2,j} - \mathbf{F}_{i-1/2,j}] - \frac{\Delta t}{\Delta y}[\mathbf{G}_{i,j+1/2} - \mathbf{G}_{i,j-1/2}], \tag{59}$$

where $\mathbf{U}^n_i$ is the integral average of $\mathbf{U}$ in cell i at timelevel n and $\mathbf{F}_{i+1/2,j}$ and $\mathbf{G}_{i,j+1/2}$ are intercell fluxes. The operator forms of the fluxes $f_{i+1/2,j}$ given by (56) apply directly to give fluxes $\mathbf{F}_{i+1/2,j}$ for the conservative form (59), i.e.,

$$\mathbf{F}_{i+1/2,j} = \mathbf{L}^{\mathrm{WAF}}_{x,\Delta t/2}(\mathbf{L}^{\mathrm{GOD}}_{y,\Delta t/2}(\mathbf{U}^n_{i,j}), \mathbf{L}^{\mathrm{GOD}}_{y,\Delta t/2}(\mathbf{U}^n_{i+1,j})). \tag{60}$$

This is to be interpreted as follows. First apply the Godunov operator $\mathbf{L}^{\mathrm{GOD}}_{y,\Delta t/2}$ to the data $\mathbf{U}^n$ at each point (i, j) to obtain an intermediate state $\mathbf{U}^G$. Second, apply the WAF operator $\mathbf{L}^{\mathrm{WAF}}_{x,\Delta t/2}$ to the state $\mathbf{U}^G$ at each intercell boundary $(i + \frac{1}{2}, j)$ to obtain the intercell fluxes $\mathbf{F}_{i-1/2,j}$. See Fig. 8 for an illustration of how $\mathbf{F}_{i+1/2,j}$ is calculated. Similarly, from (57), we have

$$\mathbf{G}_{i,j+1/2} = \mathbf{L}^{\mathrm{WAF}}_{y,\Delta t/2}(\mathbf{L}^{\mathrm{GOD}}_{x,\Delta t/2}(\mathbf{U}^n)_{i,j}, \mathbf{L}^{\mathrm{GOD}}_{x,\Delta t/2}(\mathbf{U}^n)_{i,j+1}). \tag{61}$$

This has a similar interpretation to (60). First apply the Godunov operator $\mathbf{L}^{\mathrm{GOD}}_{x,\Delta t/2}$ to the data $\mathbf{U}^n$ at each point (i, j) to obtain an intermediate state $\mathbf{U}^F$. Second, apply the WAF operator $\mathbf{L}^{\mathrm{WAF}}_{y,\Delta t/2}$ to the state $\mathbf{U}^F$ at each intercell boundary $(i, j + \frac{1}{2})$ to obtain the intercell fluxes $\mathbf{G}_{i,j-1/2}$.

For the calculation of the "predictor" states $\mathbf{U}^F$, $\mathbf{U}^G$ we suggest a robust but inexpensive Riemann solver be used, such as the HLL Riemann solver [12, 35]; for the WAF operator $\mathbf{L}^{\mathrm{WAF}}_{s,dt}$ it may be necessary to use a more accurate Riemann solver to ensure that features such as contacts and slip lines are resolved adequately. For details of Riemann solvers see [33–35]. Note that any operator that gives the Lax–Wendroff flux on the one-dimensional linear advection equation could be used instead of $\mathbf{L}^{\mathrm{WAF}}_{s,dt}$.

3.2.2. *An Average State Scheme*

It is important to note here that the formulation of the scheme presented in the last section is certainly not unique. One of many possible alternative formulations is now given. Consider again the intercell flux (44) for the second-order scheme on the linear advection equation. It can be written as

$$\begin{aligned} f_{i+1/2,j} = {} & \frac{a}{2}(2 - \nu_y)\left[\frac{1}{2}(1 + \nu_x)u^n_{i,j} + \frac{1}{2}(1 - \nu_x)u^n_{i+1,j}\right] \\ & + \frac{a}{2}\nu_y\left[\frac{1}{2}(1 + \nu_x)u^n_{i,j-1} + \frac{1}{2}(1 - \nu_x)u_{i+1,j-1}\right]. \end{aligned} \tag{62}$$

Consideration of the terms in square brackets in (62) leads us to define a weighted average state (WAS) operator based on the solution to the Riemann problem for two given states $\mathbf{Z}_L$ and $\mathbf{Z}_R$, similar to the (WAF) operator (52) but with an integral across *states* rather than *fluxes*:

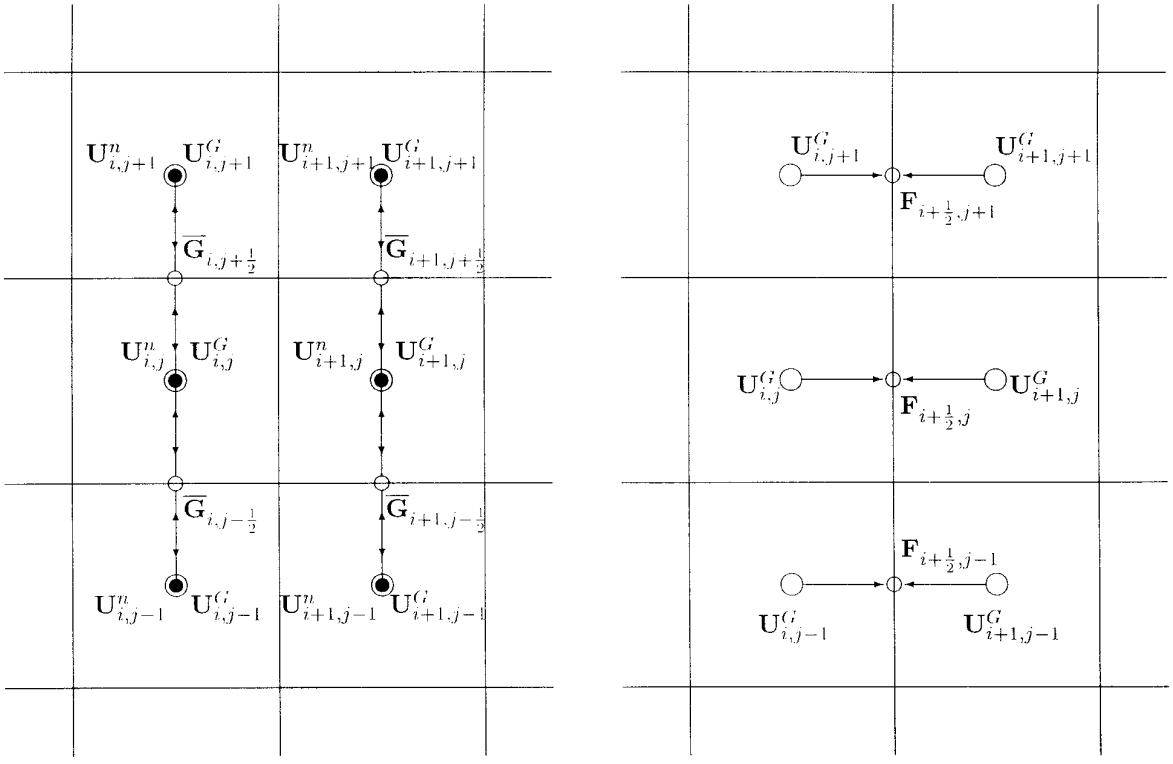

FIG. 8. Illustration of the steps involved in the calculation of intercell fluxes $\mathbf{F}_{i+1/2,j}$ for the average flux scheme of Section 3.2.1.

$$\mathbf{L}^{\mathrm{WAS}}_{s,dt}(\mathbf{Z}_L, \mathbf{Z}_R) = \frac{1}{\Delta s}\int_{-\Delta s/2}^{\Delta s/2} \mathbf{Z}^*\left(\frac{s}{dt}\right) ds. \tag{63}$$

As for the WAF operator (52) all waves in the solution to $RP(\mathbf{Z}_L, \mathbf{Z}_R)$ would be represented by single ray waves and the operator can be written as a weighted average of the states $\mathbf{Z}^{(k)}$ in the solution to the Riemann problem:

$$\mathbf{L}^{\mathrm{WAS}}_{s,dt}(\mathbf{Z}_L, \mathbf{Z}_R) = \sum_{k=1}^{N+1} W^{(k)}\mathbf{Z}^k. \tag{64}$$

The weights $W^{(k)}$ are taken as the weights (54) for the TVD version of the one-dimensional WAF scheme. Note that for the linear advection equation with the limiter function $\phi^{(k)} \equiv \nu_s$ for $s = x$ and $dt = \frac{1}{2}\Delta t$, $\mathbf{L}^{\mathrm{WAS}}_{s,dt}(u_L, u_R)$ becomes

$$\mathbf{L}^{\mathrm{WAS}}_{x,\Delta t/2}(u_L, u_R) = \tfrac{1}{2}(1+\nu_x)u_L + \tfrac{1}{2}(1-\nu_x)u_R. \tag{65}$$

Therefore, after some manipulation, the flux (62) can be written in operator form as

$$\mathbf{F}_{i+1/2,j} = \mathbf{F}(\mathbf{L}^{\mathrm{GOD}}_{y,\Delta t/2}(\mathbf{L}^{\mathrm{WAS}}_{x,\Delta t/2}(\mathbf{U}^n_{i,j}, \mathbf{U}_{i+1,j}))). \tag{66}$$

This operator form of the flux should be interpreted as follows. First apply the WAS operator to all pairs $(\mathbf{U}^n_{i,j}, \mathbf{U}_{i+1,j})$ to give an intermediate state $\hat{\mathbf{U}}$ on boundaries $(i+\frac{1}{2}, j)$. Second, compute Godunov "intercell" fluxes $\hat{\mathbf{G}}_{i+1/2,j+1/2}$, based on $\hat{\mathbf{U}}$ at *nodes* $(i+\frac{1}{2}, j+\frac{1}{2})$ and apply the Godunov operator with these fluxes to $\hat{\mathbf{U}}$ to obtain a second intermediate state $\mathbf{U}^{n+1/2}$ on the intercell boundaries. Finally, compute the flux on each of these states to give the required intercell fluxes. See Fig. 9 for an illustration of how $\mathbf{F}_{i+1/2,j}$ is calculated. The flux $\mathbf{G}_{i,j+1/2}$ corresponding to (66) is

$$\mathbf{G}_{i,j+1/2} = \mathbf{G}\,(\mathbf{L}^{\mathrm{GOD}}_{x,\Delta t/2}(\mathbf{L}^{\mathrm{WAS}}_{y,\Delta t/2}(\mathbf{U}^n_{i,j}, \mathbf{U}_{i,j+1}))). \tag{67}$$

This "average state" scheme should be cheaper than the average flux scheme described above because less flux evaluations are involved. It has not yet been tried in practice.

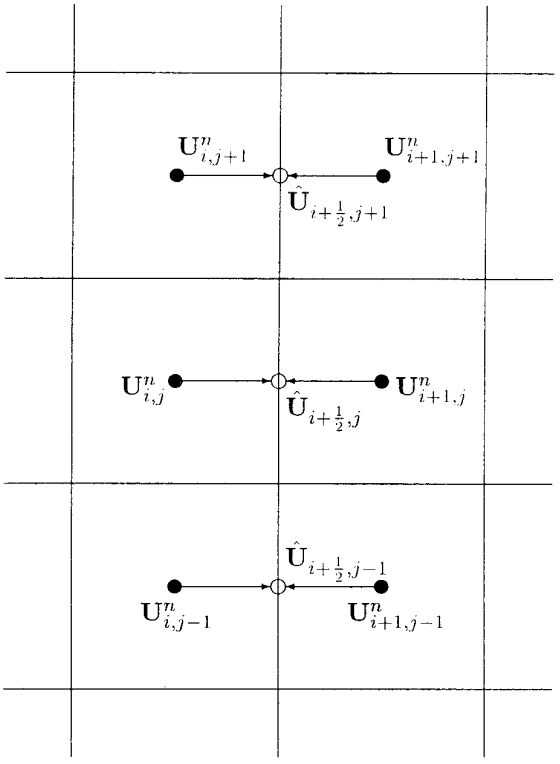

Step 1: Apply the WAS operator $\mathbf{L}^{WAS}_{x,\frac{1}{2}\Delta t}$ to data $\mathbf{U}^n$ to calculate weighted average intermediate states $\hat{\mathbf{U}}_{i+\frac{1}{2},j}$ at boundaries $(i+\frac{1}{2}, j)$.

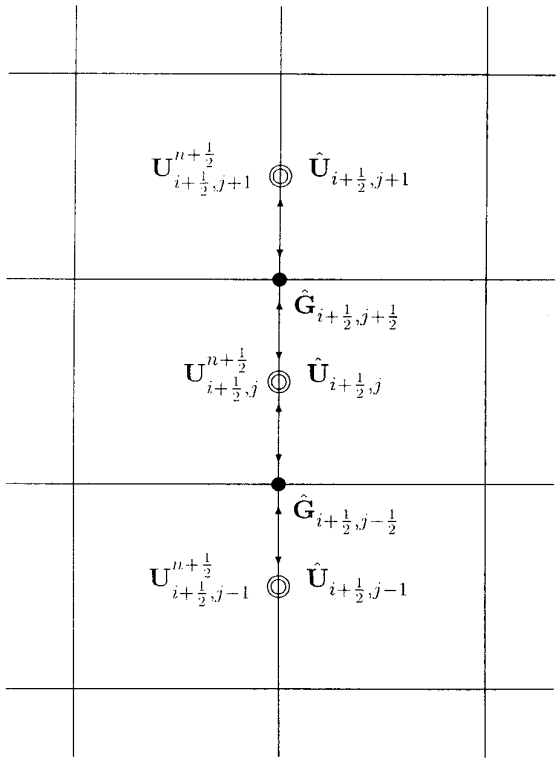

Step 2: Use the intermediate state $\hat{\mathbf{U}}$ to calculate Godunov intercell fluxes $\hat{\mathbf{G}}_{i+\frac{1}{2},j+\frac{1}{2}}$ at *nodes* $(i+\frac{1}{2}, j+\frac{1}{2})$ and use these fluxes to update $\hat{\mathbf{U}}$ to $\hat{\mathbf{U}}^{n+\frac{1}{2}}$.

FIG. 9. Illustration of the steps involved in the calculation of intercell fluxes $\mathbf{F}_{i+1/2,j}$ for the average flux scheme of Section 3.2.2. After step 2, set $\mathbf{F}_{i+1/2,j} = \mathbf{F}(\mathbf{U}^{n+1/2}_{i+1/2,j})$.

4. THE WAF APPROACH IN THREE SPACE DIMENSIONS

We now extend the two-dimensional WAF-type schemes of the last section to the linear advection equation in three space dimensions,

$$u_t + f_x + g_y + h_z = 0, \tag{68}$$

where $f = au$, $g = bu$, and $h = cu$ are flux functions. We assume here the wavespeed components a, b, and c are constant and positive.

A general WAF intercell flux in three space dimensions can be defined in an analogous way to the two-dimensional flux (30). We define the flux $\mathbf{e}_A$ across boundary A as

$$\mathbf{e}_A = \frac{1}{t_2 - t_1}\frac{1}{V(I)}\int_{t_1}^{t_2}\int_I \mathbf{e}\cdot\mathbf{n}\, dx\, dy\, dz\, dt, \tag{69}$$

where I is the three-dimensional space integration range, $V(I)$ is the volume of I, $\mathbf{e} = (au, bu, cu)$ is the general flux function, and $\mathbf{n}$ is the outward facing unit vector normal to the boundary.

4.1. Generation of Schemes on Cartesian Grids

As in the two-dimensional case, we consider the case of Cartesian grids. Let Δx, Δy, and Δz be the grid spacing, and let Δt be the timestep. We use the conservative formula in the form

$$\begin{aligned} u^{n+1}_{i,j,k} = u^n_{i,j,k} &- \frac{\Delta t}{\Delta x}\left[f_{i+1/2,j,k} - f_{i-1/2,j,k}\right] \\ &- \frac{\Delta t}{\Delta y}\left[g_{i,j+1/2,k} - g_{i,j-1/2,k}\right] - \frac{\Delta t}{\Delta z}\left[h_{i,j,k+1/2} - h_{i,j,k-1/2}\right], \end{aligned} \tag{70}$$

where $f_{i+1/2,j,k}$, $g_{i,j+1/2,k}$, and $h_{i,j,k+1/2}$ are the intercell fluxes

in the x, y, and z directions, respectively. From (69), $f_{i+1/2,j,k}$ can be written as

$$f_{i+1/2,j,k} = \frac{1}{t_2 - t_1}\frac{1}{V(I)}\int_{t_1}^{t_2}\int_I f(u^*(x, y, z, t))\, dx\, dy\, dz\, dt, \tag{71}$$

where u^* is the exact solution to Eq. (68) with the data u^n at time level n as initial conditions. The fluxes $g_{i,j+1/2,k}$ and $h_{i,j,k+1/2}$ follow similarly. As the space integration range for $f_{i+1/2,j,k}$, we consider the natural extension of the space integration used in two dimensions, which can be written as

$$I = [-\tfrac{1}{2}\Delta x, \tfrac{1}{2}\Delta x] \times [0, \Delta y] \times [0, \Delta z]. \tag{72}$$

The integration ranges for $g_{i,j+1/2,k}$ and $h_{i,j,k+1/2}$ follow by symmetry. Define also the directional Courant numbers as $\nu_x = a\Delta t/\Delta x$, $\nu_y = b\Delta t/\Delta y$, and $\nu_z = c\Delta t/\Delta z$. We assume all three to be less than unity.

The choice of integration range and Courant numbers restricts the number of states influencing $f_{i+1/2,j,k}$ to a maximum of eight: $u_{i,j,k}$, $u_{i+1,j,k}$, $u_{i,j-1,k}$, $u_{i+1,j-1,k}$, $u_{i,j,k-1}$, $u_{i+1,j,k-1}$, $u_{i,j-1,k-1}$, and $u_{i+1,j-1,k-1}$. These are arranged in the eight corners of a cube and can be considered as the initial conditions for a three-dimensional Riemann problem for (68). The exact solution to this problem is

$$u(x, y, z, t) = u^{(0)}(x - at, y - bt, z - ct), \tag{73}$$

where $u^{(0)}(x, y, z)$ is the initial data.

4.1.1. *A Second-Order Scheme*

We consider first a second-order scheme. Working from the experience of the two-dimensional case, we use the midpoint rule in time and exact integration in all three space directions. The flux in the x direction becomes

$$f_{i+1/2,j,k} = \frac{1}{V(I)}\int_I f(u^*(x, y, z, \tfrac{1}{2}\Delta t))\, dx\, dy\, dz. \tag{74}$$

Figure 10 shows the integration range I divided into the regions occupied by different fluxes at time $\frac{1}{2}\Delta t$. Performing the integral gives the flux as

$$\begin{aligned} f_{i+1/2,j,k} = {} & \tfrac{1}{8}(1 + \nu_x)(2 - \nu_y)(2 - \nu_z) f_{i,j,k} \\ & + \tfrac{1}{8}(1 - \nu_x)(2 - \nu_y)(2 - \nu_z) f_{i+1,j,k} \\ & + \tfrac{1}{8}(1 + \nu_x)\nu_y(2 - \nu_z) f_{i,j-1,k} \\ & + \tfrac{1}{8}(1 - \nu_x)\nu_y(2 - \nu_z) f_{i+1,j-1,k} \\ & + \tfrac{1}{8}(1 + \nu_x)(2 - \nu_y)\nu_z f_{i,j,k-1} \\ & + \tfrac{1}{8}(1 - \nu_x)(2 - \nu_y)\nu_z f_{i+1,j,k-1} \\ & + \tfrac{1}{8}(1 + \nu_x)\nu_y\nu_z f_{i,j-1,k-1} + \tfrac{1}{8}(1 - \nu_x)\nu_y\nu_z f_{i+1,j-1,k-1}. \end{aligned} \tag{75}$$

The fluxes $g_{i,j+1/2,k}$ and $h_{i,j,k+1/2}$ follow by symmetry. Substituting the fluxes into the conservative formula (71) gives a scheme with a 20-point compact stencil, which is not reproduced here for reasons of space. It can be shown, via truncation error analysis, that schemes of the form

$$u_{i,j,k}^{n+1} = \sum_{\alpha,\beta,\gamma} A_{\alpha,\beta,\gamma} u_{i+\alpha,j+\beta,k+\gamma}^{n} \tag{76}$$

for the three-dimensional linear advection equation (68) on regular Cartesian grids are pth-order accurate in space and time if and only if

$$\sum_{\alpha,\beta,\gamma} \alpha^q \beta^r \gamma^s A_{\alpha,\beta,\gamma} = (-\nu_x)^q (-\nu_y)^r (-\nu_z)^s \tag{77}$$

for all integer triples (q, r, s) such that $q \geq 0$, $r \geq 0$, $s \geq 0$, and $q + r + s \leq p$. See [4] for proof. Application of these conditions to the scheme resulting from flux (75) shows it to be second-order accurate in space and time.

From the experience of the equivalent scheme in two space dimensions, we expected the stability condition for this scheme to be

$$\max\{\nu_x, \nu_y, \nu_z\} \leq 1. \tag{78}$$

However, after computing the von Neumann amplification coefficient at many thousands of points, it seems that this is not sufficient by itself. For given ν_z, we can calculate the stability function $st(\nu_x, \nu_y)$ as defined in the last section. Six of these ''slices'' are shown in Fig. 11, for $\nu_z = 0.0$, 0.25, 0.5, 0.75, 1.0, 1.25. When $\nu_z = 0.0$, the scheme resulting from (76) reduces to the two-dimensional scheme (45), and the stability condition is therefore the same as for that scheme in this case. However, as ν_z increases, an area around the point $\nu_z = 1$, $\nu_y = 1$ is lost to the unstable region. When $\nu_z \geq 1$, the stability region vanishes, as expected. We have not yet been able to work out what the exact stability region is; however, if we insist on the condition (78) and add the condition

$$\nu_x + \nu_y + \nu_z \leq 2 \tag{79}$$

then any points satisfying both appear to be stable. We have calculated the von Neumann factor for many thousands of points within the region (78), (79) and found none to be unstable. From Fig. 11, we believe, however, that these conditions are only sufficient, and not necessary, for stability.

4.1.2. *The First-Order Scheme*

To construct our final scheme, we need a monotonicity preserving first-order scheme. We now present a version of the first-order scheme (41) for the three-dimensional

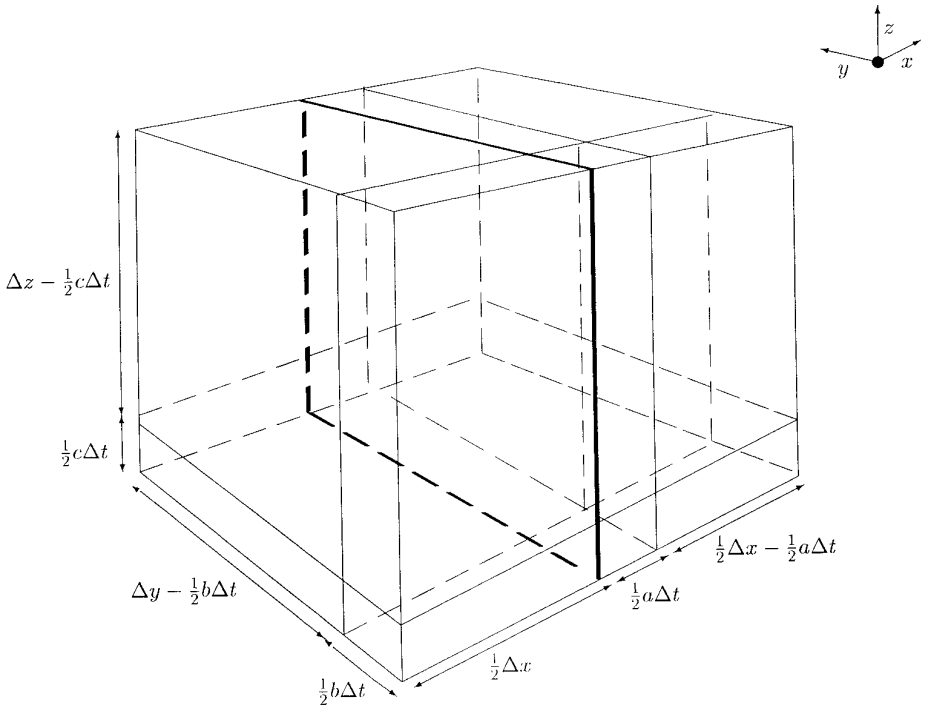

FIG. 10. Integration for the 3D scheme: midpoint rule in time; exact integration in all space directions. The status of the space integration range at time $t = \frac{1}{2}\Delta t$.

linear equation (68). This can be done by using the midpoint rule in time, the midpoint rule in space perpendicular to the boundary, and exact integration in space in both directions parallel to the boundary. See Fig. 12. The intercell flux then becomes

$$f_{i+1/2,j,k} = \frac{1}{\Delta y\,\Delta z}\int_{I\cap\{x=0\}} f(u(0,y,z,\frac{1}{2}\Delta t))\,dy\,dz. \qquad (80)$$

This can be written explicitly as

$$\begin{aligned} f_{i+1/2,j,k} = {} & \tfrac{1}{4}(2-\nu_y)(2-\nu_z)f_{i,j,k} + \tfrac{1}{4}\nu_y(2-\nu_z)f_{i,j-1,k} \\ & + \tfrac{1}{4}(2-\nu_y)\nu_z f_{i,j,k-1} + \tfrac{1}{4}\nu_y\nu_z f_{i,j-1,k-1}. \end{aligned} \qquad (81)$$

The other fluxes, $g_{i,j+1/2,k}$ and $h_{i,j,k+1/2}$, follow by symmetry. Substituting these into the conservative formula (71) gives a scheme with an eight-point stencil. Application of the accuracy conditions (77) shows this scheme to be first-order accurate. The scheme is monotonicity preserving under

$$\max\{\nu_x, \nu_y, \nu_z\} \le \tfrac{2}{3} \qquad (82)$$

since all the coefficients are positive under this condition, but this condition may not be necessary for monotonicity. Condition (82) may turn out to be the stability condition for the scheme, although numerical experiments indicate that this scheme has the same stability region as the second-order scheme presented above. Note that the scheme resulting from (81) is *not* the three-dimensional CTU scheme as derived by Colella's approach [8] in two dimensions, as might have been expected.

4.2. Extension to Nonlinear Systems

It is easy to see that (75) can be written as

$$f_{i+1/2,j,k} = \tfrac{1}{2}(1+\nu_x)f(u^{(gh)}_{i,j,k}) + \tfrac{1}{2}(1-\nu_x)f(u^{(gh)}_{i+1,j,k}), \qquad (83)$$

where

$$\begin{aligned} u^{(gh)}_{i,j,k} = {} & \tfrac{1}{4}(2-\nu_y)(2-\nu_z)u_{i,j,k} + \tfrac{1}{4}\nu_y(2-\nu_z)u_{i,j-1,k} \\ & + \tfrac{1}{4}(2-\nu_y)\nu_z u_{i,j,k-1} + \tfrac{1}{4}\nu_y\nu_z u_{i,j-1,k-1}. \end{aligned} \qquad (84)$$

If the two-dimensional Godunov operators (50), (51) are extended to three space dimensions in the obvious way, the calculation of $u^{(gh)}_{i,j,k}$ can be written as a product of two of these:

$$u^{(gh)}_{i,j,k} = \mathbf{L}^{\mathrm{GOD}}_{y,\Delta t/2}(\mathbf{L}^{\mathrm{GOD}}_{z,\Delta t/2}(u^n_{i,j,k})_{i,j,k}). \qquad (85)$$

Obviously, the Godunov operators could be reversed. The

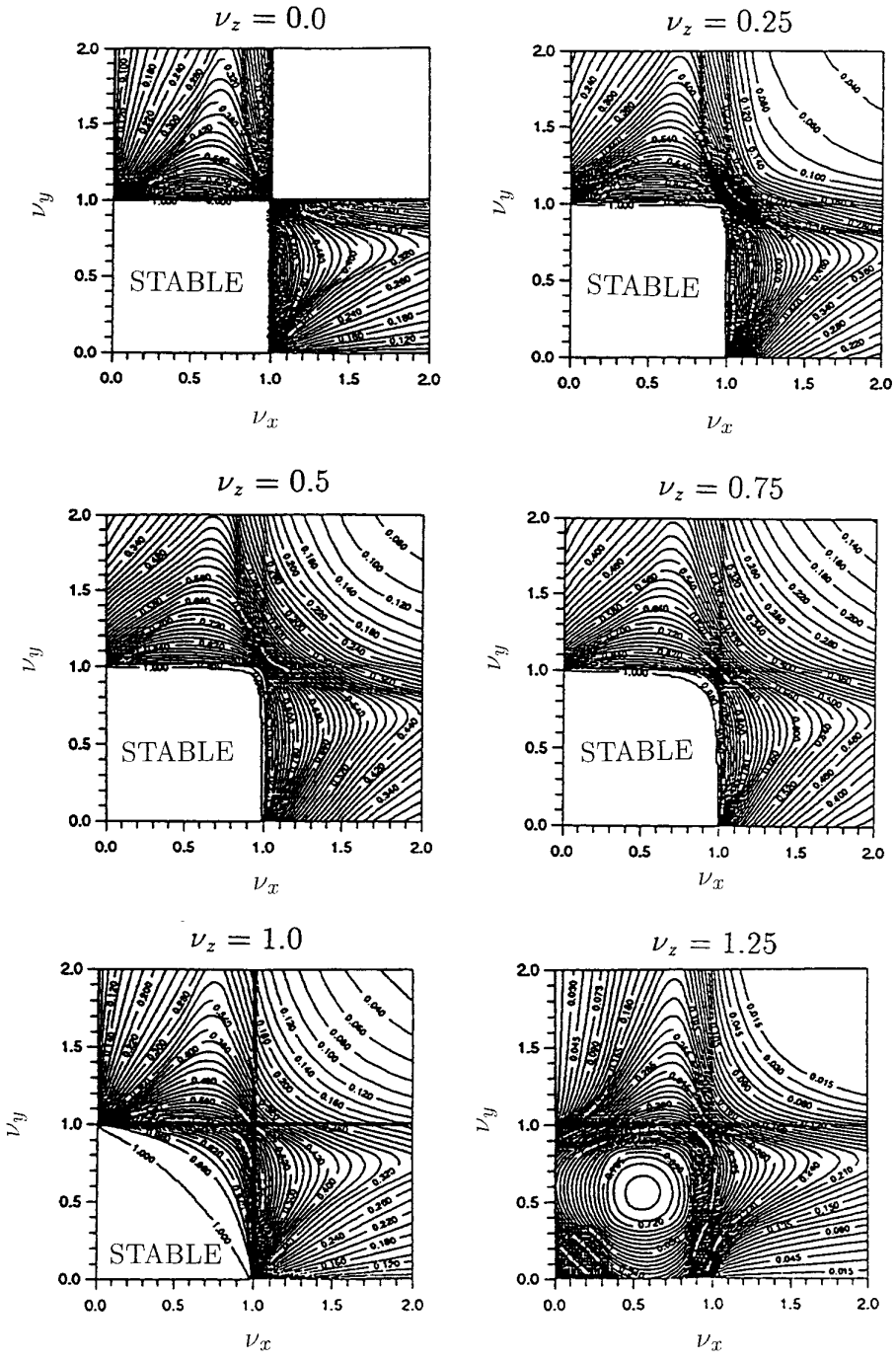

FIG. 11. Ratio of the number of stable phase angle pairs to the total number of phase angle pairs for the second-order scheme resulting from flux (75).

calculation of the flux (83) is then the WAF operator (52) applied to the pair $(u^{(gh)}_{i,j,k}, u^{(gh)}_{i+1,j,k})$ so we can write the flux as

$$f_{i+1/2,j,k} = \mathbf{L}^{\mathrm{WAF}}_{x,\Delta t/2}(\mathbf{L}^{\mathrm{GOD}}_{y,\Delta t/2}(\mathbf{L}^{\mathrm{GOD}}_{z,\Delta t/2}(u^n_{i,j,k})_{i,j,k}), \mathbf{L}^{\mathrm{GOD}}_{y,\Delta t/2}(\mathbf{L}^{\mathrm{GOD}}_{z,\Delta t/2}(u^n_{i+1,j,k})_{i+1,j,k})). \quad (86)$$

As in the two-dimensional case, the scheme can be extended to nonlinear hyperbolic systems of hyperbolic conservation laws

$$\mathbf{U}_t + \mathbf{F}(\mathbf{U})_x + \mathbf{G}(\mathbf{U})_y + \mathbf{H}(\mathbf{U})_z = 0, \quad (87)$$

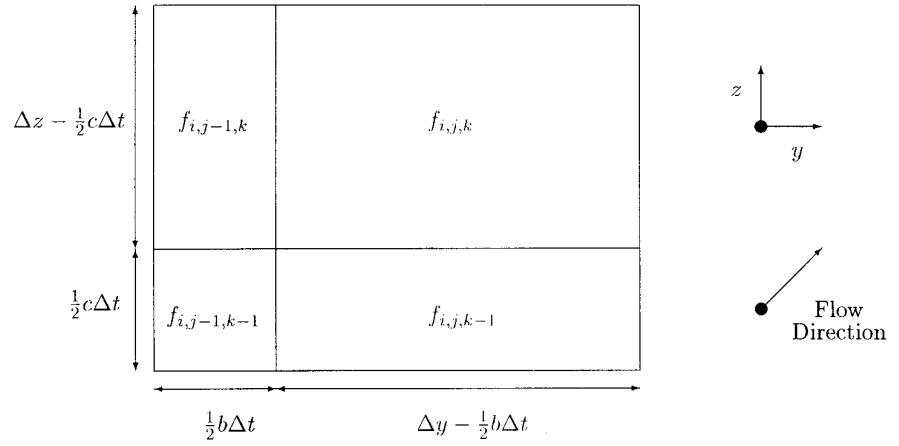

FIG. 12. Integration range for $f_{i+1/2,j,k}$ for the first-order scheme in three dimensions: midpoint rule in time, midpoint rule perpendicular to the boundary, and exact integration in both directions parallel to the boundary.

where $\mathbf{U}$ is a vector of N conserved variables and $\mathbf{F}$, $\mathbf{G}$, and $\mathbf{H}$ are vector-valued flux functions. The flux (86) can easily be extended to obtain a flux $\mathbf{F}_{i+1/2,j,k}$ for the conservative formula

$$\begin{aligned}\mathbf{U}_{i,j,k}^{n+1} = \mathbf{U}_{i,j,k}^{n} &- \frac{\Delta t}{\Delta x}\left[\mathbf{F}_{i+1/2,j,k} - \mathbf{F}_{i-1/2,j,k}\right] \\ &- \frac{\Delta t}{\Delta x}\left[\mathbf{G}_{i,j+1/2,k} - \mathbf{G}_{i,j-1/2,k}\right] \\ &- \frac{\Delta t}{\Delta x}\left[\mathbf{H}_{i,j,k+1/2} - \mathbf{H}_{i,j,k-1/2}\right]\end{aligned} \tag{88}$$

by reinterpreting the operators. We therefore take

$$\begin{aligned}\mathbf{F}_{i+1/2,j,k} = \mathbf{L}_{x,\Delta t/2}^{\mathrm{WAF}}(&\mathbf{L}_{y,\Delta t/2}^{\mathrm{GOD}}(\mathbf{L}_{z,\Delta t/2}^{\mathrm{GOD}}(\mathbf{U}_{i,j,k}^{n})_{i,j,k}), \\ &\mathbf{L}_{y,\Delta t/2}^{\mathrm{GOD}}(\mathbf{L}_{z,\Delta t/2}^{\mathrm{GOD}}(\mathbf{U}_{i+1,j,k}^{n})_{i+1,j,k}))\end{aligned} \tag{89}$$

$$\begin{aligned}\mathbf{G}_{i,j+1/2,k} = \mathbf{L}_{y,\Delta t/2}^{\mathrm{WAF}}(&\mathbf{L}_{x,\Delta t/2}^{\mathrm{GOD}}(\mathbf{L}_{z,\Delta t/2}^{\mathrm{GOD}}(\mathbf{U}_{i,j,k}^{n})_{i,j,k}), \\ &\mathbf{L}_{x,\Delta t/2}^{\mathrm{GOD}}(\mathbf{L}_{z,\Delta t/2}^{\mathrm{GOD}}(\mathbf{U}_{i,j+1,k}^{n})_{i,j+1,k}))\end{aligned} \tag{90}$$

$$\begin{aligned}\mathbf{H}_{i,j,k+1/2} = \mathbf{L}_{z,\Delta t/2}^{\mathrm{WAF}}(&\mathbf{L}_{x,\Delta t/2}^{\mathrm{GOD}}(\mathbf{L}_{y,\Delta t/2}^{\mathrm{GOD}}(\mathbf{U}_{i,j,k}^{n})_{i,j,k}), \\ &\mathbf{L}_{x,\Delta t/2}^{\mathrm{GOD}}(\mathbf{L}_{y,\Delta t/2}^{\mathrm{GOD}}(\mathbf{U}_{i,j,k+1}^{n})_{i,j,k+1})).\end{aligned} \tag{91}$$

Obviously, the Godunov operators can be reversed in these three fluxes.

This scheme is a natural extension of the "average flux" scheme presented in Section 3.2.1. The two-dimensional "average state" scheme presented in Section 3.2.2 can be extended to three space dimensions in an analogous way.

5. NUMERICAL EXPERIMENTS

We now present some numerical results from the finite volume scheme presented in Section 3.2.1 applied to the two-dimensional shallow water equations

$$\begin{pmatrix}\phi\\ \phi u\\ \phi v\end{pmatrix}_t + \begin{pmatrix}\phi u\\ \phi u^2 + \frac{1}{2}\phi^2\\ \phi uv\end{pmatrix}_x + \begin{pmatrix}\phi v\\ \phi uv\\ \phi v^2 + \frac{1}{2}\phi^2\end{pmatrix}_y = 0, \tag{92}$$

where $\phi = gH$ is the geopotential, H is the total depth, $g \approx 9.81$ is the acceleration due to gravity, and u and v are the x and y components of velocity, respectively. Riemann solvers for the one-dimensional counterpart of (92) can be found in [33 or 35]. The results will be compared with results from an operator split version of the one-dimensional WAF scheme [27]. Since the finite volume scheme under consideration is second-order accurate in space and time, the second-order splitting of Strang [28] is used for a fair comparison.

The first test problem considered is radially symmetric about the center of a square domain. It can thus be compared with numerical solutions to the one-dimensional shallow water equations with a geometric source term:

$$\mathbf{U}_t + \mathbf{F}(\mathbf{U})_r = \mathbf{S}(\mathbf{U}, r), \tag{93}$$

where

$$\begin{aligned}\mathbf{U} &= \begin{pmatrix}\phi\\ \phi w\end{pmatrix}, \quad \mathbf{F}(\mathbf{U}) = \begin{pmatrix}\phi w\\ \phi w^2 + \frac{1}{2}\phi^2\end{pmatrix}, \\ \mathbf{S}(\mathbf{U}, r) &= -\begin{pmatrix}\dfrac{\phi w}{r}\\ \dfrac{\phi w^2}{r}\end{pmatrix}.\end{aligned} \tag{94}$$

Here $w = \sqrt{u^2 + v^2}$ is the radial velocity, and r is the distance from the centre of the domain. In the solutions

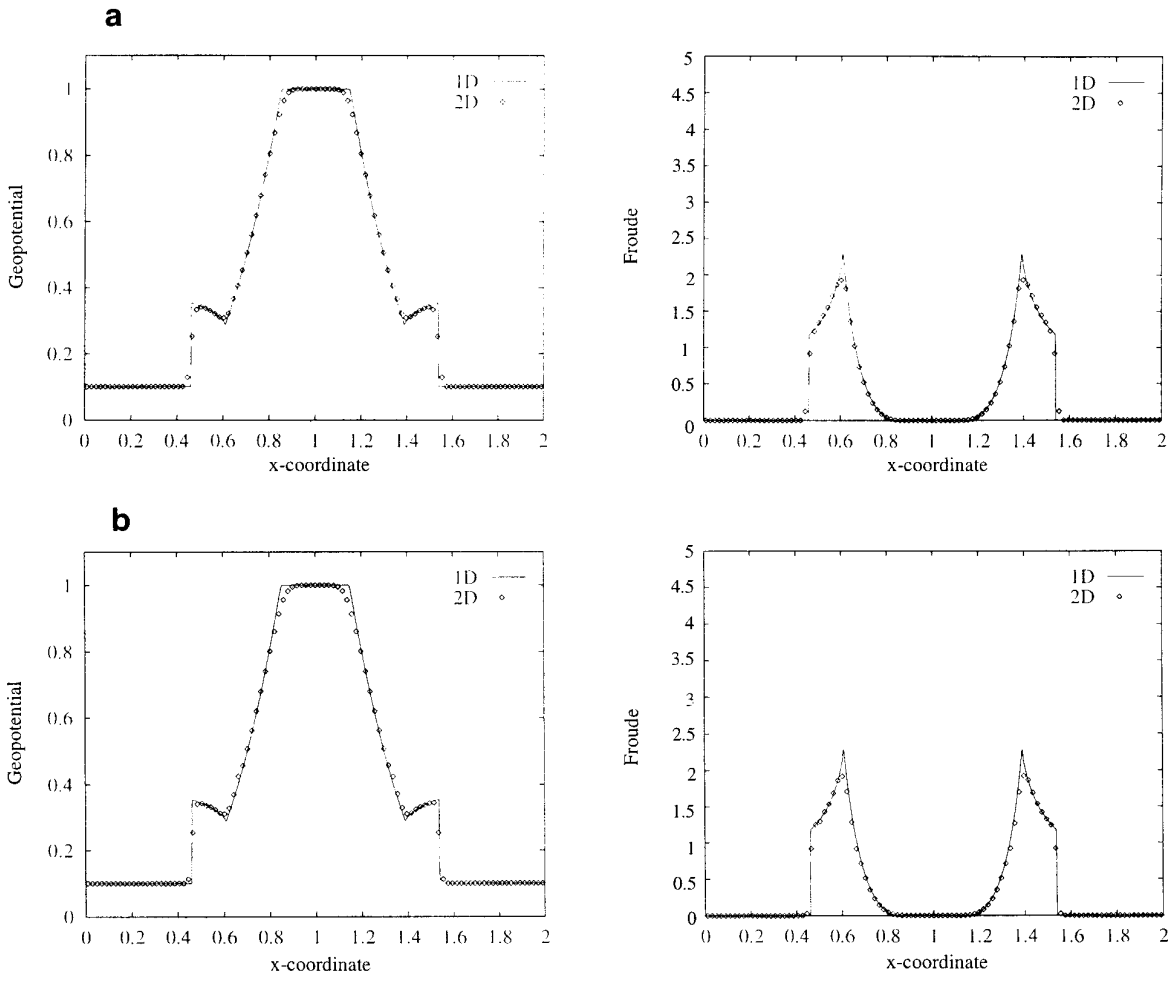

FIG. 13. Results from the explosion test: x-strips from (a) the operator split scheme and (b) the finite volume scheme of Section 3.2.1 with the van Leer limiter at time $t = 0.2$. A Courant number coefficient of 0.8 was used.

of (93), (94) presented, 2000 computational cells were used. For the initial value problem considered here, Eqs. (92) are solved within the domain $[0, 2] \times [0, 2]$ divided into 101×101 computing cells. The van Leer limiter is used in these calculations. The problem considered is a "circular dam-break problem," i.e., the initial conditions consist of two states separated by a circular discontinuity. Here the circle has radius $r = 0.35$ and is centered on the point (1,1). Any cells cut by this circle are given a weighted average of the two states, based on the relative areas of the part of the cell lying within the circle and the rest of the cell. For initial conditions, both components of velocity are set to zero everywhere and ϕ is set to 1.0 inside the circle and 0.1 outside the circle. The Courant number coefficient is set at 0.8, and results are taken at times $t = 0.2$ and $t = 0.5$. By time $t = 0.2$ a circular bore has formed and is expanding away from the center (1, 1). Within this circular bore is a circular rarefaction wave which drains fluid from the original deep region to make up for the outward movement of water caused by the progression of the bore. By time $t = 0.5$ a small dip in geopotential has formed in the central deep region caused by the reflection of the rarefaction at the center of the domain. For each solution, two cross sections are shown: a section in the plane $y = 1$, called *x-strips* here, and a section in the plane $x = y$, called *diagonal strips* here. Strips from two-dimensional solutions will always be represented by symbols in the figures; solutions to the one-dimensional equations (93), (94) are represented by solid lines. The figures show geopotential ϕ and *Froude Number*,

$$\mathbf{F} = (u^2 + v^2)/\phi.$$

Figures 13 and 14 show the x strips and diagonal strips obtained at time $t = 0.2$. Figures 15 and 16 show the equivalent results at time $t = 0.5$. These results show that the finite

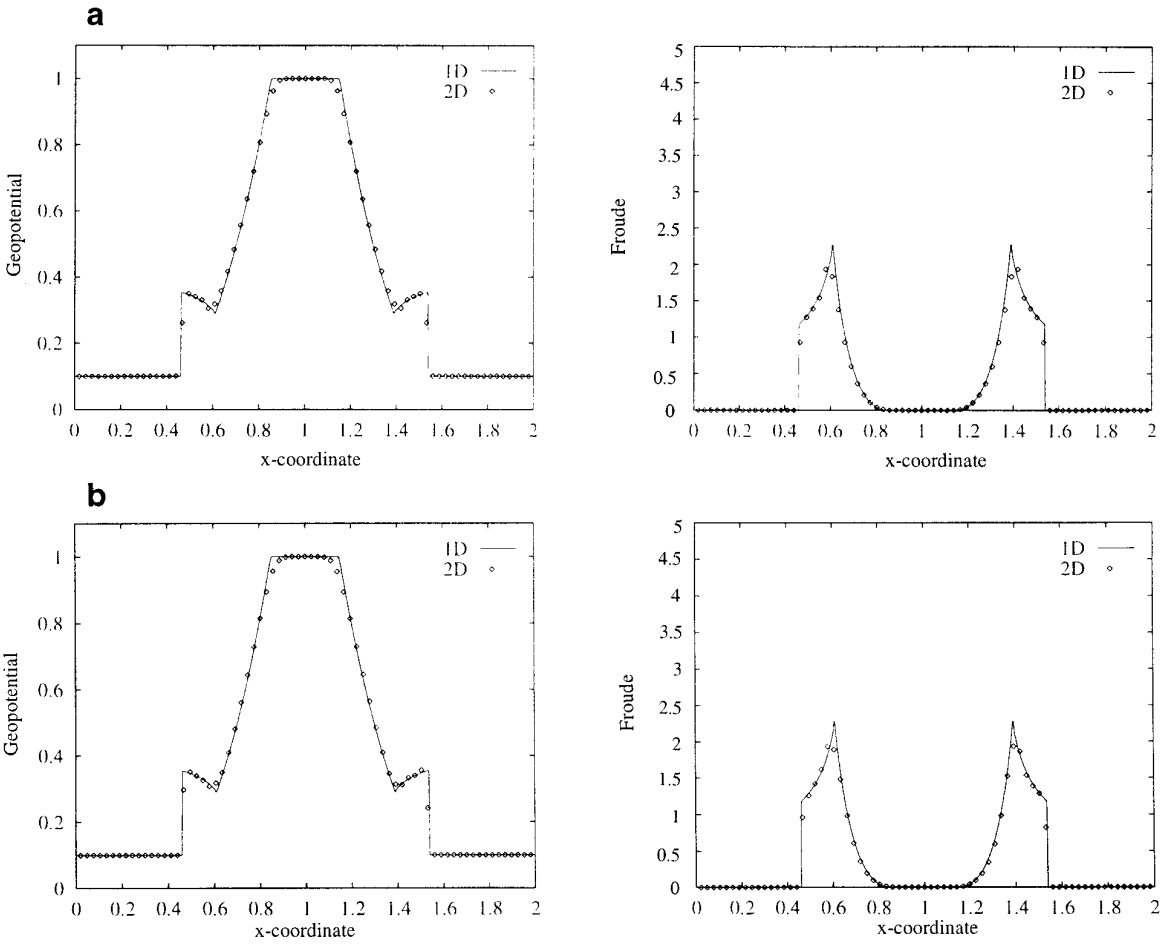

FIG. 14. Results from the explosion test: diagonal strips from (a) the operator split scheme and (b) the finite volume scheme of Section 3.2.1 with the van Leer limiter at time $t = 0.2$. A Courant number coefficient of 0.8 was used.

volume scheme tested here has resolution comparable with the operator split scheme, and is thus a competitive scheme as far as accuracy is concerned. The shocks are captured in approximately two mesh cells for the x-strips. There is no evidence of spurious oscillations in the finite volume solutions, which implies that one-dimensional TVD limiter functions are adequate for controlling these oscillations. Smooth parts of the solutions also agree well with the one-dimensional radial solution. Note, however, that the finite volume scheme fails to resolve the dip in geopotential at $x = 1$, $y = 1$ at time $t = 0.5$ as well as the operator split scheme.

The finite volume scheme has been extended for use on curvilinear grids, as described in [4]. We now present a numerical solution generated by the curvilinear version of the scheme. The problem we consider is the reflection of a bore wave from a solid boundary. This is the shallow water equivalent of the reflection of a shock wave from a solid boundary in gas dynamics. It is well known in that field that when a shock wave is reflected obliquely from a solid boundary, two main types of reflection can occur: *regular reflection* and *Mach reflection.* In regular reflection, just two shock waves exist—the incident shock and a reflected shock. These two shocks meet at the boundary. In Mach reflection, the incident and reflected shocks meet at the *triple point* with a third shock wave called the *Mach stem*, which joins this point to the boundary. A slip line extends from the triple point into the region of smooth flow between the Mach stem and the reflected shock. Various types of Mach reflection are possible. If the reflection is exactly as described above, it is called *single Mach reflection* (SMR); *complex Mach reflection* (CMR) is the same as SMR except with a kink in the reflected shock; *double Mach reflection* (DMR) is the same as CMR except that a second Mach stem appears between the kink in the reflected shock and the slip line. See the book by Ben-Dor [3] for details of the physics behind shock reflection in gas dynamics.

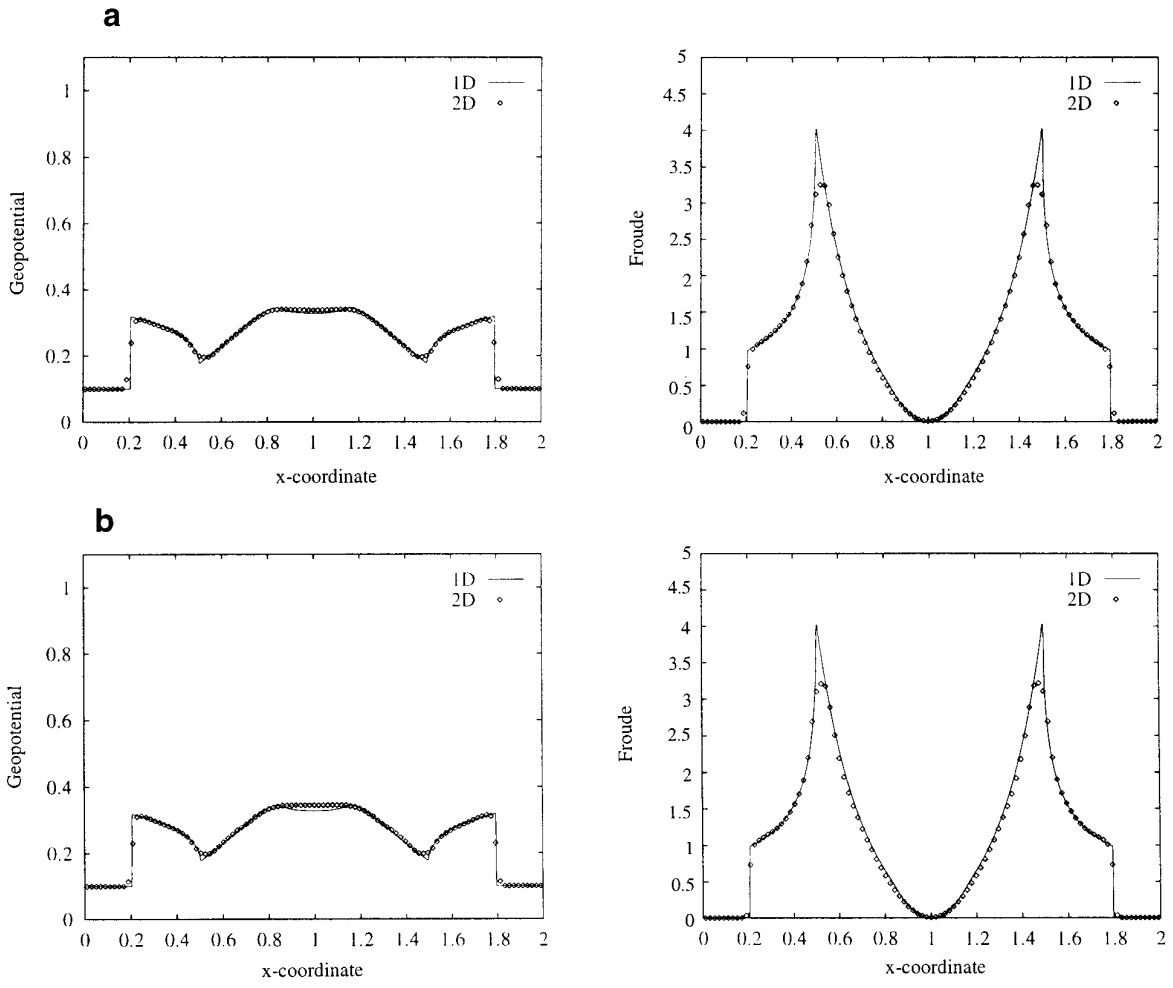

FIG. 15. Results from the explosion test: x-strips from (a) the operator split scheme and (b) the finite volume scheme of Section 3.2.1 with the van Leer limiter at time $t = 0.5$. A Courant number coefficient of 0.8 was used.

It seems to be less well known that Mach reflection of bore waves can occur in shallow water. The only recent papers in which the phenomena is discussed appear to be Krehl *et al.* [13] and Takayama *et al.* [29]. We first note that a bore wave travelling in the x direction from left to right in two space dimensions is completely determined by the state $(\phi_R, u_R, 0)$ ahead of the bore and the *bore Froude number*

$$F_S = \frac{S^2}{\phi_R}, \tag{95}$$

where S is the speed of the bore. Conditions that determine the state (ϕ_L, u_L, v_L) behind the bore can be found by applying the Rankine–Hugoniot condition

$$\Delta \mathbf{F} = S\,\Delta \mathbf{U} \tag{96}$$

to the shallow water equations. They can be summarised as follows. Define

$$r = \tfrac{1}{2}(-1 + \sqrt{1 + 8(\sqrt{F_R} - \sqrt{F_S})^2}), \tag{97}$$

where $F_R = u_R^2/\phi_R$ is the Froude number of the pre-bore state. The postbore state is then determined as

$$\phi_L = r \cdot \phi_R \tag{98}$$

$$u_L = S + \frac{1}{r}(u_R - S) \tag{99}$$

$$v_L = v_R = 0, \tag{100}$$

where $S = \sqrt{\phi_R F_S}$ from (95).

A bore with a Froude number of 8.0 travelling into a prebore state,

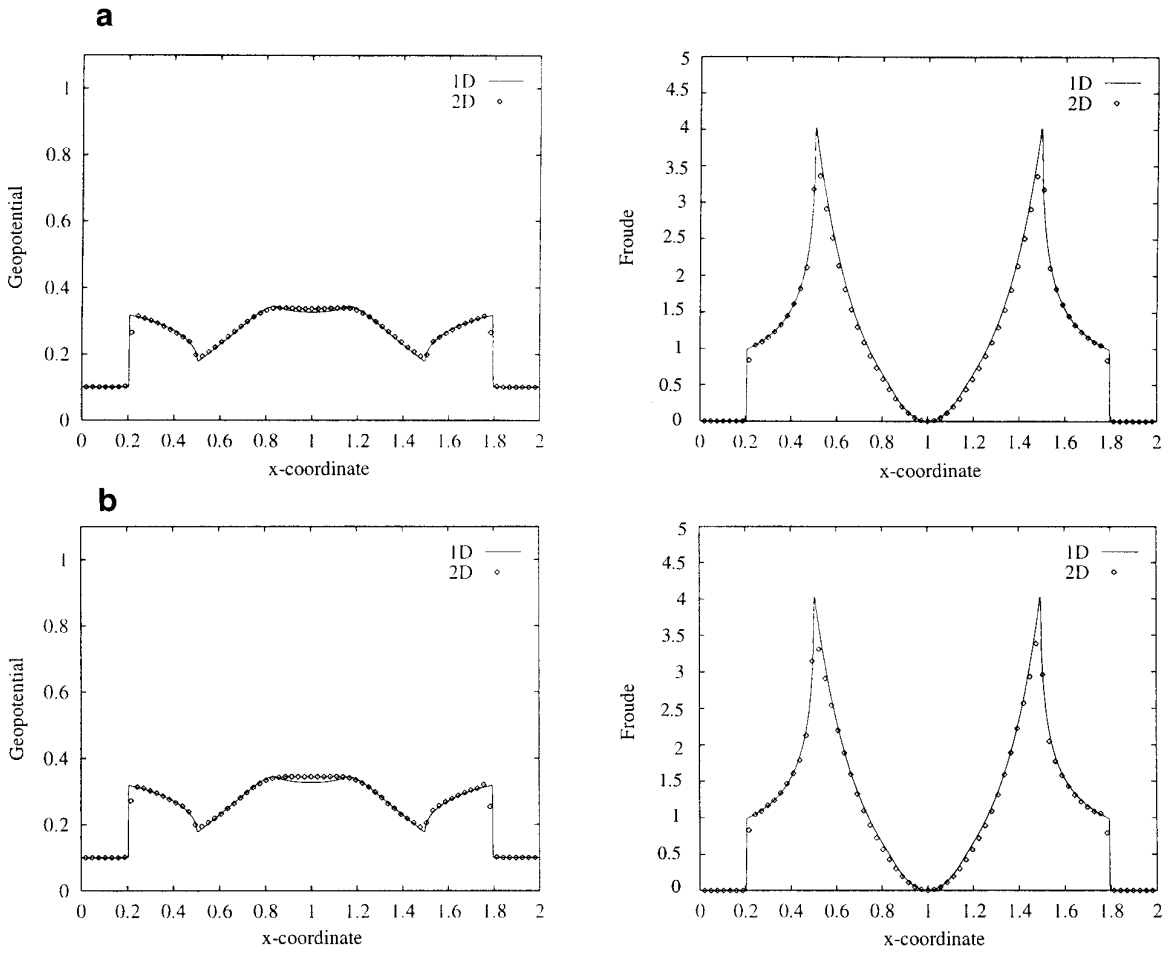

FIG. 16. Results from the explosion test: diagonal strips from (a) the operator split scheme and (b) the finite volume scheme of Section 3.2.1 with the van Leer limiter at time $t = 0.5$. A Courant number coefficient of 0.8 was used.

$$(\phi_R, u_R, v_R) = (1.0, 0.0, 0.0), \tag{101}$$

and reflecting from a boundary at an angle of 40° to its direction of travel is considered here. The type of curvilinear grid used in the calculations is shown in Fig. 17. The actual grid used was much finer than the picture, having 400×400 cells. The Courant number coefficient was set at 0.8 and a MINMOD-type limiter function [33] was used. The exact Riemann solver [33, 35] was used everywhere except in the predictor stages of the finite volume scheme, where the HLL solver [12, 33] was used. Note, however, that any approximate Riemann solver could have been used instead of the exact Riemann solver. See [33, 35], for details of various Riemann solvers and their implementation.

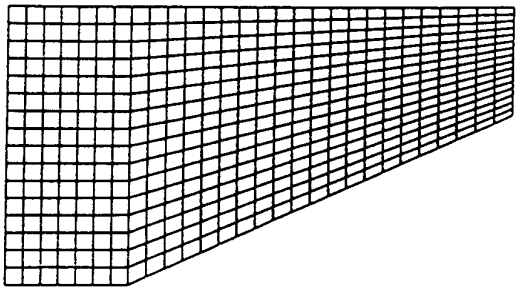

FIG. 17. An illustration of the grid type used in the bore reflection calculations.

Plots of geopotential ϕ and Froude number are shown for each reflection. The results of the operator split scheme are shown in Fig. 18; the results of the finite volume scheme are shown in Fig. 19. The schemes indicate that this reflection is a CMR, since a kink appears in the reflected bore. There is a glitch in the operator split result which is large enough to have deformed the Mach stem near the wall. This does not appear in the finite volume result. More work is needed

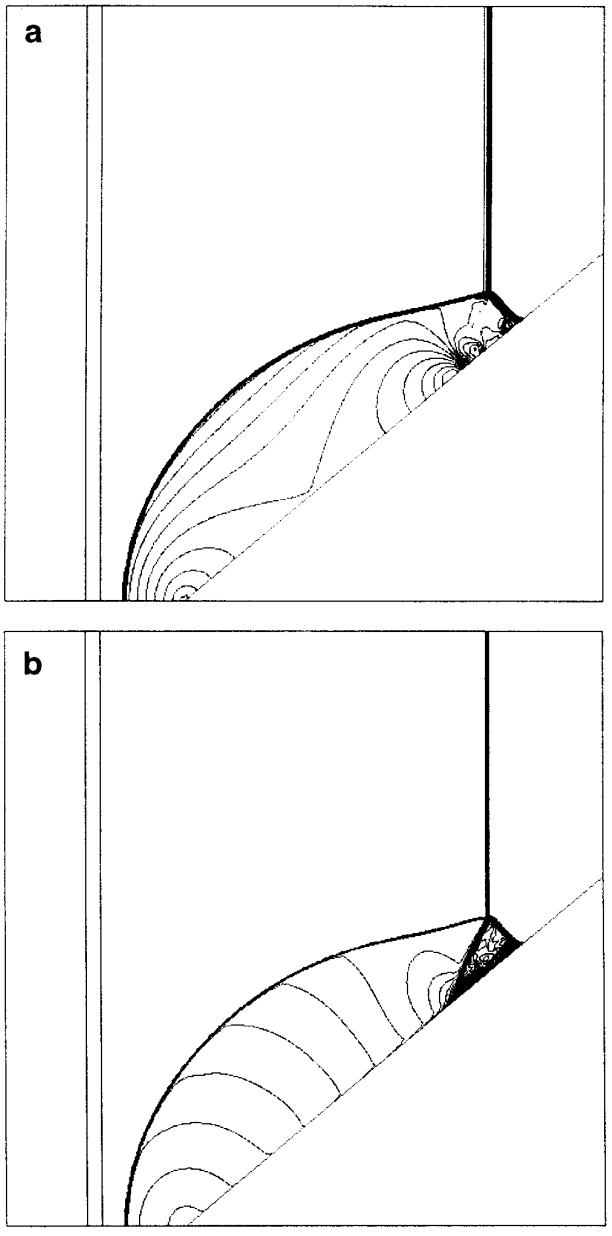

FIG. 18. Reflection of a bore of Froude number 8.0 over a 40° wedge using the operator split scheme. Part (a) shows the geopotential and part (b) shows the Froude number.

here to establish the reason for the difference between these results, and experimental results are needed for comparison.

Approximate timings have indicated that the finite volume scheme with the HLL Riemann solver on the predictor steps is approximately 20% cheaper than the one dimensional WAF scheme combined with the Strang splitting (i.e., three sweeps), if the split scheme uses the same Riemann solver as the final stages of the finite volume flux calculations.

6. SUMMARY

The aim of this paper has been to present the WAF approach in the context of other schemes in the literature and illustrate its potential for generating new schemes, particularly in two and three dimensions. Our methods are, by definition, conservative and for appropriate integration schemes they are also second-order accurate in space and

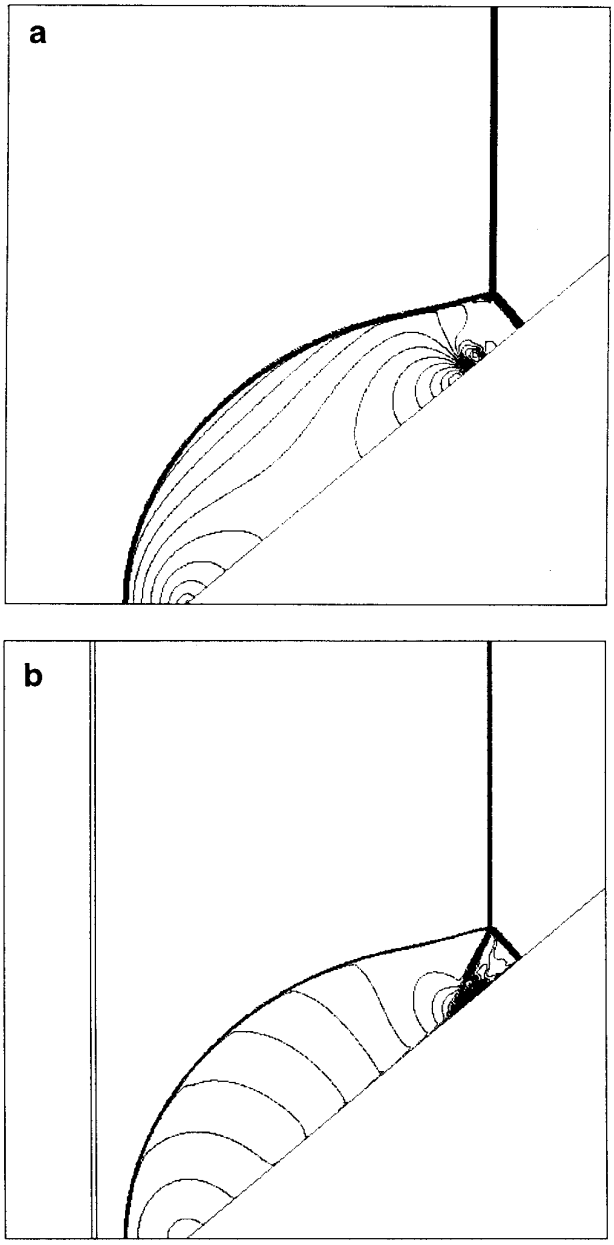

FIG. 19. Reflection of a bore of Froude number 8.0 over a 40° wedge using the finite volume scheme of Section 3.2.1. Part (a) shows the geopotential and part (b) shows the Froude number.

time. In one dimension, we showed how well-known schemes such as the Lax–Wendroff scheme [14], the Warming–Beam scheme [44], the MUSCL Hancock scheme [42], the PLM scheme of Colella [7], and the GRP method of Ben-Artzi and Falcovitz [2] can be described in terms of the WAF approach. In two space dimensions, we reproduced the first-order CTU scheme of Colella [8] and used the approach to derive two finite volume schemes that are second-order accurate in space and time. As far as we know, these schemes are new. They have multidimensional upwinding aspects and numerical experiments suggest good stability properties. As an indication of their practical use, we showed how one of these schemes could be extended to nonlinear systems in two ways, to produce an ''average flux'' scheme and an ''average state'' scheme. Spurious oscillations are controlled in both schemes by the use of one-dimensional TVD limiter functions. Some numerical results were presented for the ''average flux'' scheme applied to the two-dimensional shallow water equations. We went on to derive the equivalent first- and second-order schemes for the three-dimensional linear advection equation, and extended them to produce an ''average flux'' scheme for three-dimensional nonlinear systems of hyperbolic conservation laws.

ACKNOWLEDGMENTS

The authors thank Phil Roe for useful comments on an early version of this paper, and Bill Speares for his invaluable contribution to early discussions on the ideas presented here. The choice of the Mach reflection problem was motivated by discussions with Kazu Takayama, to whom the authors are indebted. Much of the work presented here was done while the first named author was a SERC-supported Ph.D student at the College of Aeronautics, Cranfield University, Cranfield, Bedfordshire, MK43 OAL, England, UK. The authors are indebted to Ed Boden for providing the one-dimensional shallow water code with geometric source terms.

REFERENCES

1. M. J. Baines, Multidimensional upwinding, in *Numerical Methods for Wave Propagation Phenomena*, edited by E. F. Toro, J. F. Clarke, and D. M. Causon (Kluwer Academic, New York, 1996).
2. M. Ben-Artzi and J. Falcovitz, *J. Comput. Phys.* **55,** 1 (1985).
3. G. Ben-Dor, *Shock Wave Reflection Phenomena* (Springer-Verlag, New York/Berlin, 1992).
4. S. J. Billett, Ph.D thesis, College of Aeronautics, Cranfield University, UK, 1994.
5. S. J. Billett and E. F. Toro, ''Numerical Methods for Overlapping Grids and Moving Boundaries,'' in *Sixth International Symposium on Computational Fluid Dynamics*, *Lake Tahoe*, *NV*, *September 1995*, Vol. I, pp. 111–116.
6. S. J. Billett and E. F. Toro, ''TVB Limiter Functions for Multidimensional Schemes,'' in *Sixth International Symposium on Computational Fluid Dynamics*, *Lake Tahoe*, *NV*, *September 1995*, Vol. I, pp. 117–122.
7. P. Colella, *SIAM J. Sci. Stat. Comput.* **6,** 104 (1985).
8. P. Colella, *J. Comput. Phys.* **87,** 171 (1990).
9. S. K. Godunov, *Mat. Sb.* **47,** 271 (1959).
10. J. B. Goodman and R. J. LeVeque, *Math. Comput.* **45**(21), 15 (1985).
11. A. Harten, *SIAM J. Numer. Anal.* **21**(1), (1984).
12. A. Harten, P. D. Lax, and B. van Leer, *SIAM Rev.* **25**(1), 35 (1983).
13. P. Krehl and M. van der Geest, *Shock Waves* **1,** 3 (1991).
14. P. Lax and P. Wendroff, *Comm. Pure Appl. Math.* **13,** 217 (1960).
15. P. D. Lax and B. Wendroff, *Comm. Pure Appl. Math.* **17,** 381 (1964).
16. R. J. LeVeque, *J. Comput. Phys.* **78,** 36 (1988).
17. R. J. LeVeque, ''Simplified Multidimensional Flux Limiter Methods,'' in *Numerical Methods in Fluid Dynamics 4: Proceedings, 1992 International Conference on Numerical Methods in Fluids, Reading, 1993,* edited by M. J. Baines and K. W. Morton, p. 173.
18. S. Osher and F. Solomon, *Math. Comput.* **38**(158), 339 (1982).
19. J. J. Quirk, *Comput. Fluids* **23**(1), 125 (1994).
20. P. L. Roe, *J. Comput. Phys.* **43,** 357 (1981).
21. P. L. Roe, Technical Report 81047, Royal Aircraft Establishment, Bedford, England, 1981 (unpublished).
22. P. L. Roe, ''The Use of the Riemann Problem in Finite Difference Schemes,'' in *Proceedings, Seventh International Conference on Numerical Methods in Fluid Dynamics, 1981,* p. 354.
23. P. L. Roe, Some contributions to the modelling of discontinuous flows, *Lect. Appl. Math.* **22,** 163 (1985).
24. P. L. Roe, Discrete models for the numerical analysis of time-dependent multidimensional gas dynamics, *J. Comput. Phys.* **63,** 458 (1986).
25. P. L. Roe, The Harten memorial lecture: Novel applications of upwind methods, in *Numerical Methods for Wave Propagation Phenomena*, edited by E. F. Toro, J. F. Clarke, and D. M. Causon, (Kluwer Academic, Amsterdam, 1996).
26. C. W. Schulz-Rinne, J. P. Collins, and H. M. Glaz, Numerical solution of the Riemann problem for two dimensional gas dynamics, *SIAM J. Sci. Stat.* **14**(6), 1394 (1993).
27. W. Speares and E. F. Toro, A high resolution algorithm for time-dependent shock dominated problems with adaptive mesh refinement, *J. Flight Sci. Space Res.,* to appear.
28. G. Strang, On the construction and comparison of difference schemes, *SIAM J. Numer. Anal.* **5**(3), 506 (1968).
29. K. Takayama, Y. Miura, M. Olim, T. Saito, and E. F. Toro, Mach reflection of water waves in conjunction with tsunami at the Okushir Island, in *Symposium on Shock Waves, Tokyo, Japan, Jan. 1994.*
30. E. F. Toro, Technical Report 8708, Cranfield CoA, 1986 (unpublished).
31. E. F. Toro, A weighted average flux method for hyperbolic conservation laws, *Proc. R. Soc. London A* **423,** 401 (1989).
32. E. F. Toro, Riemann-problem based techniques for computing reactive two-phase flows, in *Proc. Third Intern. Confer. on Numerical Combustion, Antibes*, *France*, *May 1989*, edited by Dervieux and Larrouturrou, Lect. Notes in Phys., Vol. 351 (Springer-Verlag, New York/Berlin, 1989), p. 472.
33. E. F. Toro, Riemann problems and the WAF method for solving two-dimensional shallow water equations, *Phil. Trans. R. Soc. London A* **338,** 43 (1992).
34. E. F. Toro, The weighted average flux method applied to the time-dependent Euler equations, *Phil. Trans. R. Soc. London A* **341,** 499 (1992).
35. E. F. Toro, *Riemann Solvers and Upwind Methods for Fluid Dynamics.* (Springer-Verlag, New York/Berlin, 1996).
36. E. F. Toro and S. J. Billett, A unified, Riemann problem based

extension of the Warming–Beam and Lax–Wendroff methods, *IMA J. Numer. Anal.,* (to appear).

37. E. F. Toro and S. J. Billett, A unified Riemann problem based extension of the Warming–Beam and Lax–Wendroff Methods, in *Proceedings, Fifth International Symposium on Computational Fluid Dynamics, Tohoku University, Sendai, Japan, September 1993*, Vol. III, edited by H. Daiguji, p. 243.
38. E. F. Toro and S. J. Billett, Technical Report 9312, Cranfield CoA, 1993 (unpublished).
39. E. F. Toro and P. L. Roe, A hybridised high-order random choice method for quasi-linear hyperbolic systems, in *Proc. 16th Intern. Symp. on Shock Tubes and Waves*, *Aachen*, *Germany*, *July 1987*, edited by Gronig, p. 701.
40. B. van Leer, Towards the ultimate conservative difference scheme IV. A new approach to numerical convection, *J. Comput. Phys.* **23,** 276 (1977).
41. B. van Leer, Towards the ultimate conservative difference scheme V. A. second order sequel to Godunov's method, *J. Comput. Phys.* **32,** 101 (1979).
42. B. van Leer, On the relation between the upwind-differencing schemes of Godunov, Enguist–Osher and Roe, *SIAM J. Sci. Stat. Comput.* **5**(1), (1985).
43. B. van Leer, Technical Report CR-189708/ICASE 92-43, NASA, Sept. 1992 (unpublished).
44. R. F. Warming and R. W. Beam, Upwind second order difference schemes with applications in aerodynamic flows, *AIAA J.* **24,** 1241 (1976).
45. P. Woodward and P. Colella, The numerical simulation of two-dimensional fluid flow with strong shocks, *J. Comput. Phys.* **54,** 115 (1984).
46. T. Zhang and Y. Zhang, Conjecture on the structure of solutions of the Riemann problem for two dimensional gas dynamics, *SIAM J. Math. Anal.* **21**(3), 593 (1990).